Cell Reports

Article

Sphingolipid paracrine signaling impairs keratinocyte adhesion to promote melanoma invasion

Graphical abstract

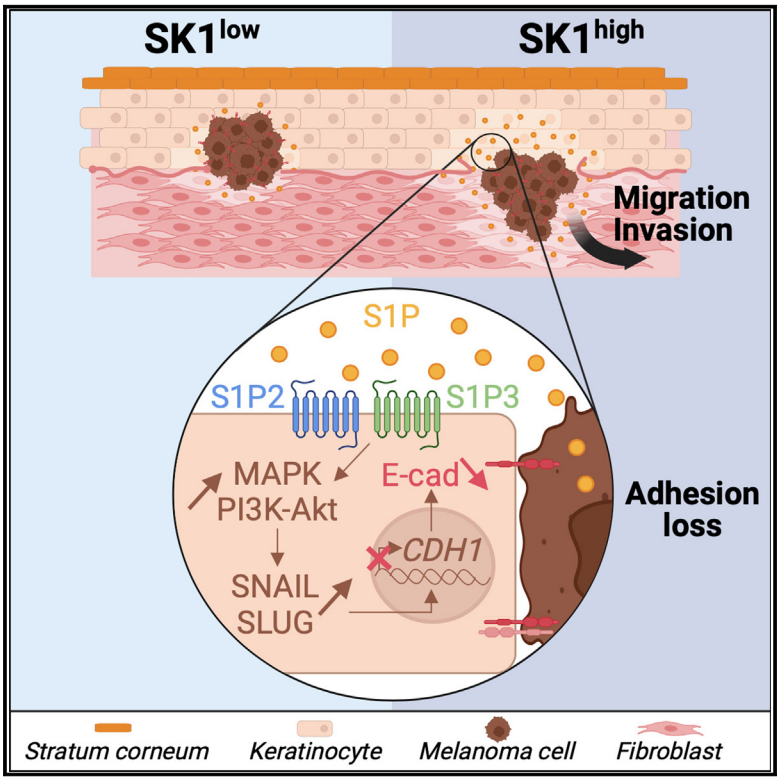

Highlights

- Primary melanoma cells overexpress sphingosine kinase 1 (SK1), the S1P-producing enzyme
- Tumor cell-derived S1P promotes melanoma cell motility in a non-cell-autonomous manner
- S1P changes keratinocyte transcriptome and adhesive function through S1P2/3 receptors
- Low epidermal E-cadherin and high tumoral SK1 correlate with invasion in primary melanomas

Authors

Justine Noujarède, Lorry Carrié, Virginie Garcia, ..., Laure Gibot, Joëlle Riond, Nathalie Andrieu-Abadie

Correspondence

nathalie.andrieu@inserm.fr

In brief

Noujarède, Carrié et al. identify sphingosine 1-phosphate (S1P), secreted by melanoma cells, as a paracrine lipid factor that reduces the adhesive properties of keratinocytes and promotes tumor invasion. Low E-cadherin expression in the epidermis, associated with high expression of S1P-producing enzymes in neighboring tumors, support the invasive potential of early-stage melanoma.

Noujarède et al., 2023, Cell Reports *42*, 113586
December 26, 2023
https://doi.org/10.1016/j.celrep.2023.113586

CellPress

Cell Reports

CellPress
OPEN ACCESS

Article

Sphingolipid paracrine signaling impairs keratinocyte adhesion to promote melanoma invasion

Justine Noujarède,[1,7] Lorry Carrié,[1,7] Virginie Garcia,[1] Maxime Grimont,[2] Anaïs Eberhardt,[2,3] Elodie Mucher,[1] Matthieu Genais,[1] Anne Schreuder,[1] Stéphane Carpentier,[1] Bruno Ségui,[1] Laurence Nieto,[1] Thierry Levade,[1,4] Susana Puig,[5] Teresa Torres,[5] Josep Malvehy,[5] Olivier Harou,[2,3] Jonathan Lopez,[2,3] Stéphane Dalle,[2,3] Julie Caramel,[2] Laure Gibot,[6] Joëlle Riond,[1,8] and Nathalie Andrieu-Abadie[1,8,9,*]

[1]Université de Toulouse, INSERM, CNRS, Université Toulouse III-Paul Sabatier, Centre de Recherches en Cancérologie de Toulouse, Toulouse, France

[2]Université Claude Bernard Lyon 1, INSERM 1052, CNRS 5286, Centre de Recherches en Cancérologie de Lyon, Lyon, France

[3]Service de Dermatologie, Hospices Civils de Lyon, Centre Hospitalier Lyon Sud, Pierre Bénite, France

[4]Laboratoire de Biochimie Métabolique, CHU de Toulouse, Toulouse, France

[5]Melanoma Unit, Department of Dermatology, University of Barcelona, Barcelona, Spain & CIBER of Rare Diseases, Instituto de Salud Carlos III, Barcelona, Spain

[6]Université Toulouse III Paul-Sabatier, Laboratoire des Interactions Moléculaires et Réactivité Chimique et Photochimique, CNRS UMR5623, Toulouse, France

[7]These authors contributed equally

[8]These authors contributed equally

[9]Lead contact

*Correspondence: nathalie.andrieu@inserm.fr

https://doi.org/10.1016/j.celrep.2023.113586

SUMMARY

Melanoma is the deadliest form of skin cancer due to its propensity to metastasize. It arises from melanocytes, which are attached to keratinocytes within the basal epidermis. Here, we hypothesize that, in addition to melanocyte-intrinsic modifications, dysregulation of keratinocyte functions could initiate early-stage melanoma cell invasion. We identified the lysolipid sphingosine 1-phosphate (S1P) as a tumor paracrine signal from melanoma cells that modifies the keratinocyte transcriptome and reduces their adhesive properties, leading to tumor invasion. Mechanistically, tumor cell-derived S1P reduced E-cadherin expression in keratinocytes via S1P receptor dependent Snail and Slug activation. All of these effects were blocked by S1P2/3 antagonists. Importantly, we showed that epidermal E-cadherin expression was inversely correlated with the expression of the S1P-producing enzyme in neighboring tumors and the Breslow thickness in patients with early-stage melanoma. These findings support the notion that E-cadherin loss in the epidermis initiates the metastatic cascade in melanoma.

INTRODUCTION

Despite organized screening programs, facilitated visual diagnosis, and accessibility of surgery, cutaneous melanoma (CM) is one of the most fatal neoplasms, mostly due to its propensity to metastasize.[1] Targeted therapy and immunotherapy are major breakthroughs in the treatment of metastatic CM but are only successful in a subset of patients and associated with severe side effects.[2] Early diagnosis remains the most efficient strategy to achieve long-term remission. However, predictive biomarkers allowing identification of CM patients at risk of metastasis are lacking.[3] To improve the clinical outcome of CM patients, it is of utmost importance to understand the molecular mechanisms underlying tumor progression before dissemination. The switch from an epithelial-like to a mesenchymal-like phenotype has been associated with CM cell invasion, but it is not considered a reliable predictive marker. Indeed, whereas a large proportion of primary CM cells show an epithelial-like phenotype with high E-cadherin expression,[4] an inverse coupling between E- and N-cadherin is not absolute in metastatic CM, with one-third of metastatic CM expressing both E- and N-cadherin.[5]

Interestingly, analysis by confocal laser-scanning microscopy of human primary malignant melanocytic lesions has shown disarray of the normal architecture of the epidermis, such as disruptions in the regular "honeycomb" pattern of keratinocytes with poorly defined cell borders.[6] Moreover, epidermal effacement, also known as consumption of the epidermis, is a histological feature that can be seen in a number of CMs.[7] However, whether and how these changes in the epidermis participate in melanomagenesis is not well known.

Our previous work has highlighted that sphingolipid metabolism is altered in human CM,[8–11] facilitating the production

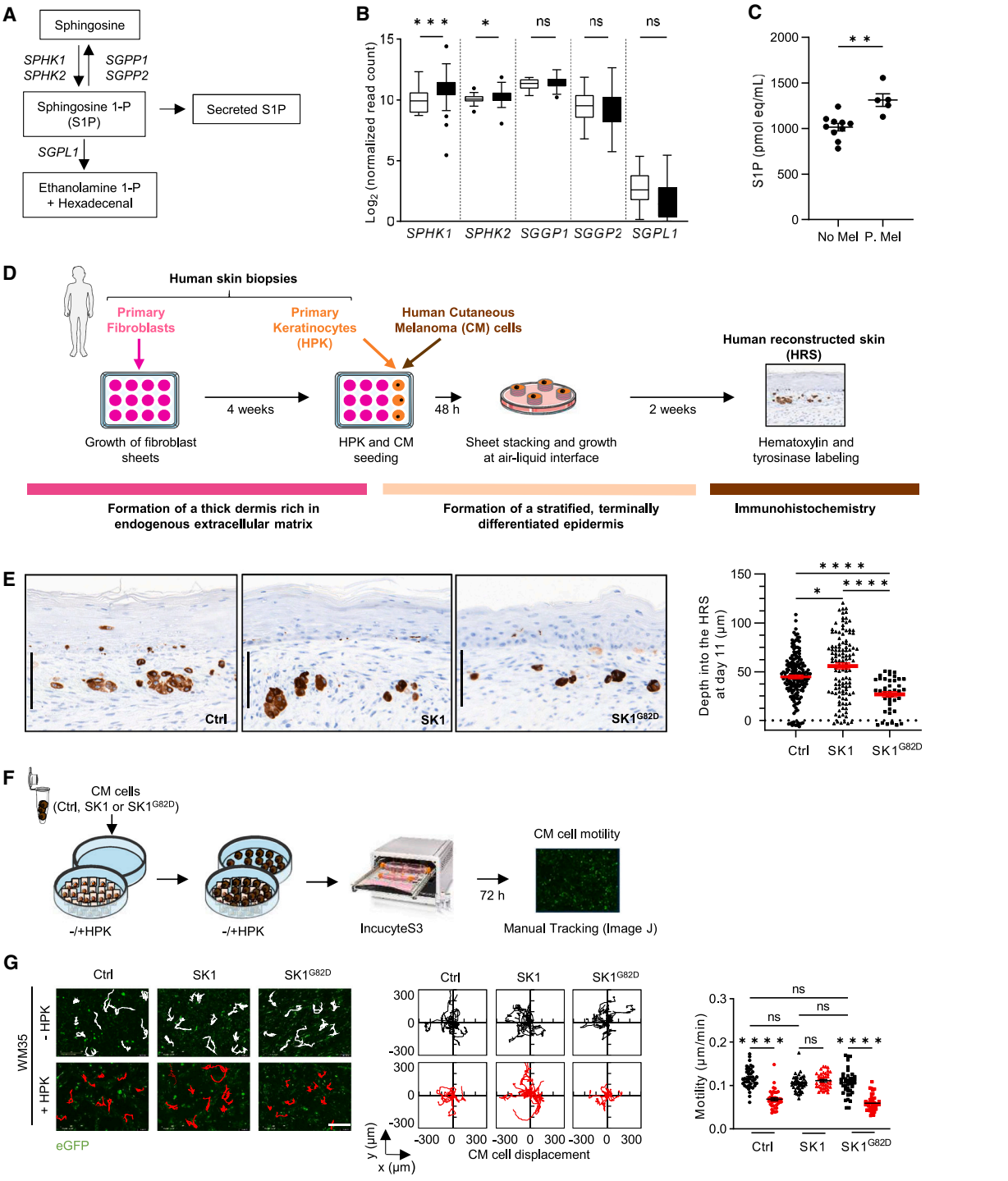

Figure 1. High SK1 activity is associated with melanoma invasion and abolishes the keratinocyte's control of melanoma motility

(A) Schematic of S1P-metabolizing enzymes.

(B) *SPHK1*, *SPHK2*, *SGPP1*, *SGPP2*, and *SGPL1* mRNA levels in human nevi (white, n = 23) and primary CM (black, n = 57), extracted from published raw data.[16]

(C) Plasma S1P levels in individuals without (No Mel, n = 10) or with primary CM (P. Mel, n = 5).

(D) Schematic of the *in vitro* formation of human reconstructed skin (HRS), including CM cells.

(E) Histological sections of HRS containing WM35 cells overexpressing or not overexpressing (control [Ctrl]) wild-type SK1 (SK1) or its catalytically inactive variant (SK1^{G82D}). Left: images of hematoxylin and tyrosinase-labeled HRS sections (scale bars, 100 µm). Right: graph reporting the distances between CM cells and the

(legend continued on next page)

Table 1. Correlations between expression of *SPHK1* and S1P transporter genes in primary melanoma tumors

Gene	Spearman's rank correlation coefficient	p Value
SPNS2	0.2317	< 0.05
	0.2844	< 0.0001
ABCA1	–	Ns
	0.2332	< 0.001
ABCC1	0.3652	< 0.01
	0.3301	< 0.0001
ABCG2	–	Ns
	–	Ns

SPHK1, *SPNS2*, *ABCA1*, *ABCC1*, and *ABCG2* mRNA levels were assessed in CM samples from the published dataset[16] (upper line, n = 57) and The Cancer Genome Atlas (TCGA) (lower line, n = 231). Correlations between *SPHK1* and S1P transporter gene expression levels were assessed using Spearman's rank-order correlation coefficient.

and secretion by tumor cells of lipid oncometabolites, such as sphingosine 1-phosphate (S1P).[8] S1P is produced by two sphingosine kinase isoenzymes, SK1 and SK2, and, after secretion, can act in the extracellular space through S1P receptors (S1PRs), a family of five specific G protein-coupled receptors (S1P1–S1P5). SK1 is considered as an oncogenic lipid kinase because it regulates tumor cell proliferation and migration as well as angiogenesis in many forms of cancer.[12,13] Interestingly, we recently reported that high expression of SK1 is significantly associated with shorter survival in melanoma patients treated with anti-PD-1.[11]

In the human epidermis, sphingolipids and S1P have both structural and biological functions.[14] Whereas ceramides play a major role in the formation of the skin barrier and the prevention of transepidermal water loss, the function of S1P in epidermal homeostasis is less understood. For instance, deletion of the S1P-specific phosphatase SPP1, which is associated with S1P accumulation in the skin of *Sgpp1*$^{-/-}$ mice, leads to epidermal abnormalities, such as altered thickness and increased expression of keratinocyte differentiation markers. In addition, S1P stimulates *in vitro* differentiation of human keratinocytes through S1P2.[15]

The role of S1P in keratinocyte behavior and function in the context of early-stage CM remains unknown. To define this role, we set up 2D cell co-cultures and 3D integrated skin models containing keratinocytes and CM cells secreting various levels of S1P. By combining multiplex immunofluorescence and digital image analysis, the epidermis neighboring early-stage tumors, isolated from patients with CM and having various levels of SK1 expression, was investigated.

RESULTS

Increased SK1 expression in early-stage melanoma cells elicits tumor invasion and impairs keratinocytes' control over tumor cell motility

Our analysis of the expression of sphingolipid-metabolizing enzymes from a published dataset comparing laser-microdissected melanocytic nevi and primary CM samples[16] revealed that malignant tumors exhibit a transcriptional up-regulation of SK1 (encoded by *SPHK1)* and, to a lesser extent, SK2 (encoded by *SPHK2*) (Figures 1A and 1B). In contrast, no significant modification was observed in the expression of S1P-degrading enzymes, such as the S1P phosphatases (encoded by *SGPP1* and *SGPP2*) and S1P lyase (encoded by *SGPL1*). In addition, our analysis showed that *SPHK1* expression correlates with that of genes encoding proteins identified as S1P membrane transporters, such as *SPNS2*[17] and *ABCC1*[18] (Table 1). These findings were confirmed by analyzing The Cancer Genome Atlas (TCGA) transcriptomics data of primary CM. No significant correlation was found for *ABCG2* (Table 1), which has also been identified as an S1P transporter.[19] Altogether, these data suggest that, in primary CM lesions, tumor cells are equipped to generate and secrete more S1P than melanocytes under normal conditions. In accordance, systemic plasma S1P levels were significantly higher in patients with primary CM compared with those in healthy individuals (Figure 1C; Table S1), with no significant variation in the concentrations of other plasma ceramide metabolites (Figure S1), suggesting that inside-out signaling of S1P is associated with melanomagenesis.

To assess the role of SK1/S1P in regulating CM cell behavior in the skin, we generated stable melanoma cell lines overexpressing either wild-type SK1 or its catalytically inactive variant SK1^{G82D} from the early-stage melanoma cell line WM35 (Figure S2A). As expected, increases in SK1 enzymatic activity and S1P secretion were observed in SK1-overexpressing cells compared with cells expressing an empty vector or SK1^{G82D} (Figures S2B and S2C). These changes or exogenous S1P exposure did not affect WM35 cell growth (Figure S2D). Then, to monitor the effect on tumor cell invasion, we set up a 3D integrated model of human reconstructed skin (HRS) containing WM35 cells, using the tissue engineering self-assembly approach[20] (Figure 1D). Interestingly, we showed an increased invasion depth of SK1-overexpressing WM35 cells into the dermis of HRS compared with control or mutant SK1-expressing WM35 cells (Figure 1E).

basal lamina. Cells with a negative distance were located in the basal layer of the epidermis. The median ± SEM is indicated (one experiment representative of two independent experiments performed in duplicates).

(F and G) Ctrl, SK1, or SK1^{G82D}-overexpressing WM35 cells were seeded alone (−HPKs) or co-cultured with keratinocytes (+HPKs). The 2D motility of EGFP-expressing CM cells (green) was monitored during 72 h by time-lapse fluorescence microscopy (Incucyte S3). Individual trajectories were manually tracked using ImageJ.

(F) Protocol.

(G) Left and center: images (scale bar, 400 μm; cell trajectories are indicated in white or red) and projections of 10 cell trajectories from one representative experiment of three. Right: graphs reporting the motility of 40 tracked CM cells. Results are expressed in micrometers per minute. The median ± SEM is indicated. Statistical significance was determined by Mann-Whitney test (B), Student's t test (C), and Kruskal-Wallis test followed by Dunn's post hoc test (E and G). (ns, not significant; *, $p < 0.05$; **, $p < 0.01$; ***, $p < 0.001$; ****, $p > 0.0001$) See also Table S1 and Figures S1 and S2.

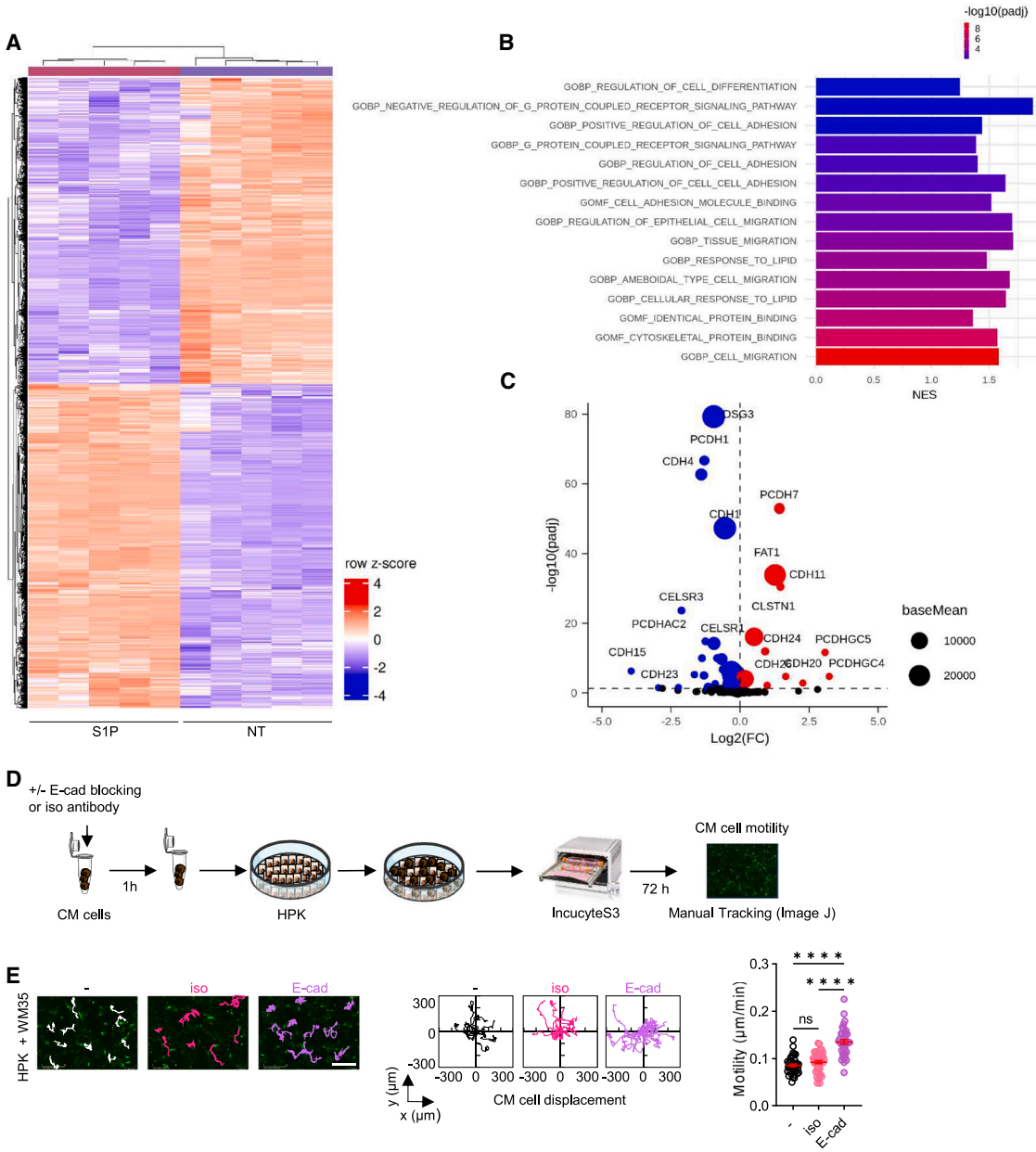

Figure 2. S1P downregulates a melanoma invasion-related cadherin in keratinocyte

(A–C) HPKs were treated with S1P (1 μM) for 24 h or left untreated and collected for RNA-seq (five replicates).

(A) Heatmap showing the non-supervised hierarchical clustering based on the differentially expressed genes (DEGs) between S1P-treated and vehicle-treated cells.

(B) Bar plot representing the normalized enrichment score (NES) of Gene Ontology (GO) terms from biological process (BP) and molecular function (MF) enriched in S1P-treated HPKs compared with untreated HPKs. Terms shown were picked from the most significant pathways (adjusted p [padj] < 0.01), and they are ordered by padj from blue (least significant) to red (most significant).

(C) Volcano plot representing cadherin-related genes in the DEGs between S1P-treated and vehicle-treated HPKs. The dotted horizontal line represents the threshold of statistical significance ($p < 0.05$). Color coding is based on the fold change (FC; red, upregulated; blue, downregulated; black, not significant). Dot size indicates mean of normalized counts for all samples.

(D and E) Ctrl WM35 cells were pre-incubated with an isotypic antibody (iso) or an E-cadherin-blocking antibody (E-cad) before being added to HPKs. The 2D motility of EGFP-expressing WM35 cells (green) was monitored during 72 h by time-lapse fluorescence microscopy. Individual trajectories were manually tracked using ImageJ.

(legend continued on next page)

Epidermal keratinocytes constitute the predominant cells of the early-stage CM microenvironment, considering their key role in regulating melanocyte behavior under physiological conditions. To examine whether tumor SK1 could regulate the interactions between keratinocytes and CM cells, WM35 cells overexpressing or not overexpressing wild-type SK1 or SK1^{G82D} were co-cultured with human primary keratinocytes (HPKs) and assayed for their 2D motility (Figure 1F). Time-lapse microscopy monitoring revealed that the motility of control WM35 cells was inhibited in the presence of HPKs compared with control WM35 cells cultured alone. In contrast, HPKs failed to impair the motility of WM35 cells overexpressing wild-type but not catalytically inactive SK1 (Figure 1G). Similar effects were observed in wound healing assays monitored by videomicroscopy (Figures S2E and S2F; Videos S1–S4). Importantly, our data also showed that SK1 overexpression (Figure 1G) or exogenous S1P exposure (Figure S2G) did not affect the motility of WM35 cells cultured alone.

Collectively, our data demonstrate that increased SK1 expression in CM cells does not enhance their motility in a cell-autonomous manner but impairs HPK functions involved in its control.

Tumor SK1/S1P induces E-cadherin loss in keratinocytes and promotes E-cadherin-expressing melanoma cell motility

To determine whether tumor cells could affect keratinocyte functions through S1P paracrine signaling, we monitored the S1P-induced changes in HPK gene expression by RNA sequencing. We identified differentially expressed genes (DEGs) using gene set enrichment analysis software (Figure 2A). This analysis validated that Gene Ontology terms associated with ''response to lipid'' and ''G protein-coupled receptor signaling pathway'' signatures were enriched in S1P-treated HPKs compared with vehicle-treated HPKs (Figure 2B). Importantly, many DEGs were significantly enriched in cell adhesion. Because cadherins are the major cell-cell adhesion molecules in the epidermis,[21] we evaluated the effect of S1P on the expression profile of the cadherin family. As shown in Figure 2C, two cadherins strongly expressed in HPKs, CDH1 and DSG3, which encode E-cadherin and desmoglein-3, respectively, were among the most significantly downregulated genes upon S1P treatment.

We focused our attention on E-cadherin because it controls the adhesion of keratinocytes to the surrounding melanocytes in the epidermis through homotypic binding between keratinocytes and CM cells.[21] To assess its role in HPKs controlling CM cell motility, WM35 cells, which express E-cadherin (Figure S3A), were incubated with an E-cadherin-blocking antibody (Figure 2D). This treatment led to increased motility of CM cells co-cultured with HPKs (Figure 2E).

Previously published immunohistochemistry studies have demonstrated that a small proportion of primary CM cells do not, or weakly, express E-cadherin.[22] To determine whether the effect of SK1 on CM motility depends on E-cadherin expression in CM cells, additional E-cadherin^{high} (G361 and M249) and E-cadherin^{low} (SbCl2 and WM1552C) CM cell lines (Figure S3B) overexpressing or not overexpressing wild-type SK1 or SK1^{G82D} were generated (Figure S2A). Increased wild-type SK1 enzymatic activity was associated with greater S1P secretion in all CM cell lines (Figures S3D and S3E). In accordance with the results obtained with WM35 cells (Figures 1G and S2G), SK1 overexpression or exogenous S1P exposure had no effect on CM cell growth (Figure S3F) or motility (Figures 3A–3D and S3G) in a cell-autonomous manner. In contrast, wild-type SK1 overexpression blocked the HPK control over CM cell motility for E-cadherin^{high} but not for E-cadherin^{low} CM cell lines (Figures 3A–3E). Moreover, E-cadherin blocking in E-cadherin^{high} CM cells restored tumor cell motility despite the presence of HPKs (Figure S3H). Altogether, we demonstrated that the HPK ability to inhibit CM cell motility as well as the non-cell autonomous effect of SK1 on CM motility were significantly correlated with E-cadherin levels in CM cells (Figures 3E and 3F).

S1P impairs keratinocyte adhesive properties through S1P2/3 receptors

To further characterize the SK1/S1P paracrine mechanism, exogenous S1P treatments were used to mimick the S1P secreted from SK1-overexpressing CM cells. Our data showed that S1P restored the motility of E-cadherin^{high} CM cells co-cultured with HPKs (Figures 4A–4D). Moreover, antagonists of S1P2 (JTE-013) and S1P3 (CAY10444) receptors, but not the one targeting the S1P1 receptor (W146), abolished S1P-induced CM motility, indicating an S1P2/3 receptor-dependent process (Figures 4A–4D). Similar effects were observed in wound healing assays monitored by videomicroscopy (Figure S4A; Videos S5–S8). In contrast, S1P had no effect on the motility of E-cadherin^{low} CM cells co-cultured with HPKs (Figures S4B and S4C).

To assess whether the S1P/S1PR axis also affects CM cell attachment to HPKs, we performed adhesion assays by incubating S1P-treated HPKs with an extended panel of E-cadherin^{high} and E-cadherin^{low} CM cells (Figures 4F and S3A–S3C). As illustrated in Figure 4G, adhesion of CM cells to S1P-treated HPKs was reduced to a greater extent in E-cadherin^{high} CM cells. Moreover, the inhibitory effect of S1P was strongly correlated with E-cadherin levels in CM cells (Figure 4H). Of note, pre-treatment of E-cadherin^{high} CM cells with an E-cadherin-blocking antibody (Figure 4F) also decreased their adhesion to HPKs (Figure 4I). Importantly, the ability of S1P to reduce cell-cell adhesion was not affected by W146 but reversed by JTE-013 and, to a lesser extent although not significantly, by CAY10444 (Figure 4J).

Collectively, our observations reveal that the tumor protein SK1, via S1P secretion and binding to S1P2/3 receptors, reprograms HPKs to function as regulators of E-cadherin^{high} CM cell attachment and spreading.

(D) Protocol.

(E) Left and center: images (scale bar, 400 μm; cell trajectories are indicated in white, pink, or purple) and projections of 10 cell trajectories from one representative experiment of three. Right: graphs reporting the motility of 40 tracked CM cells. Results are expressed in micrometers per minute; the median ± SEM is indicated. Statistical significance was determined by one-way ANOVA followed by Tukey's post hoc test. (ns, not significant; ****, $p < 0.0001$) See also Figure S3.

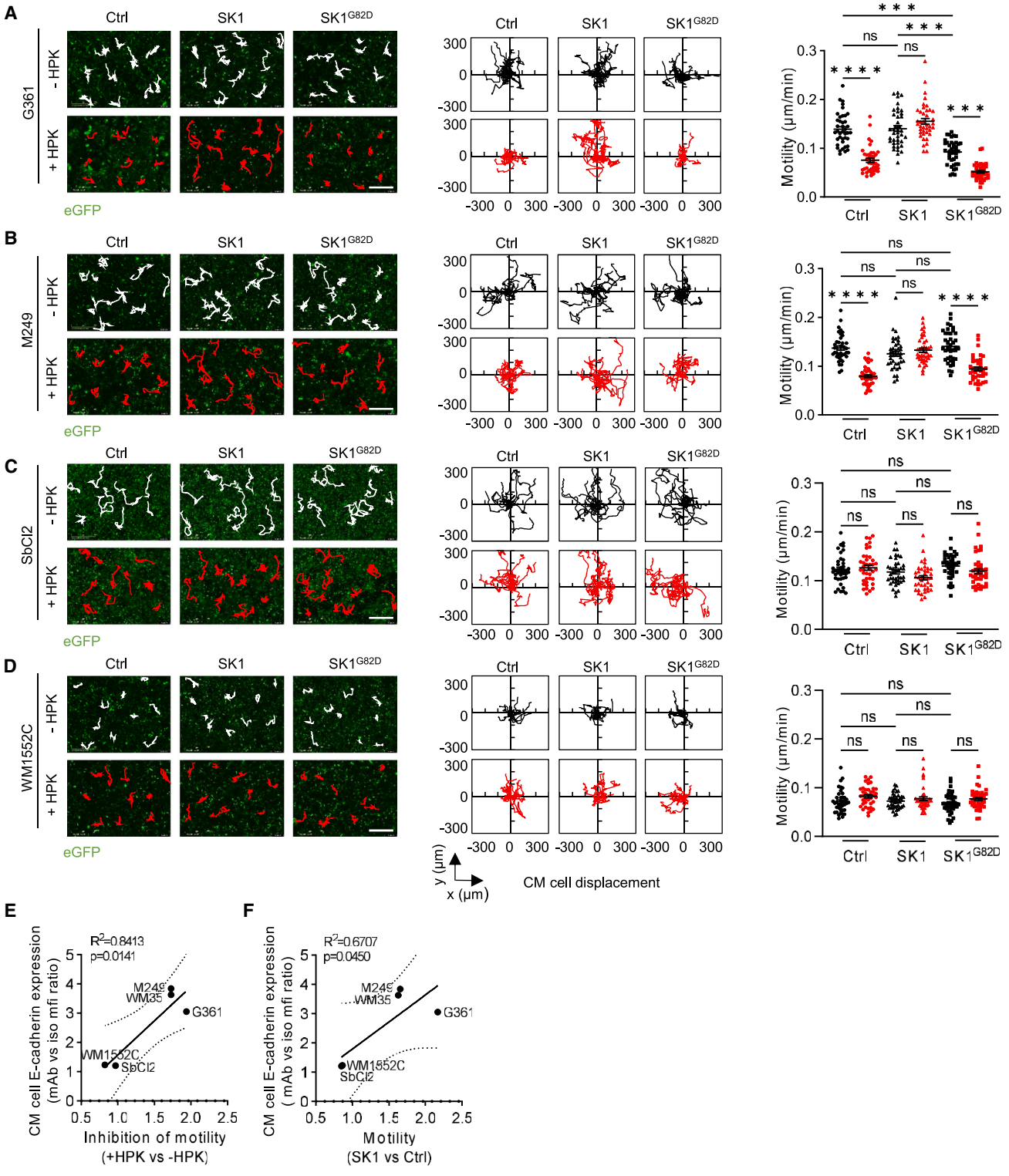

Figure 3. Tumor SK1 promotes the motility of E-cadherin^{high}, but not E-cadherin^{low}, melanoma cells

Ctrl, SK1, or SK1^{G82D}-overexpressing G361, M249, SbCl2, and WM1552C cells were seeded alone (−HPKs) or co-cultured with keratinocytes (+HPKs). The 2D motility of EGFP-expressing CM cells (green) was monitored during 72 h by time-lapse fluorescence microscopy (Incucyte S3) as described in Figure 1F. Individual trajectories were manually tracked using ImageJ.

(legend continued on next page)

S1P-induced E-cadherin loss in keratinocytes is mediated by S1P2/3 receptor-dependent signaling

In addition to *CDH1* downregulation (Figure 2C), we also identified a significant decrease of E-cadherin protein levels in HPKs upon S1P treatment (Figure 5A). This effect was inhibited by S1P2 and S1P3, but not S1P1, receptor antagonists (Figure 5A). In line with these observations, inhibitors of mitogen-activated protein kinase kinase (MEK) and phosphatidylinositol 3-kinase (PI3K)/Akt, which are both activated by the S1P/S1PR axis,[23] prevented the S1P-induced decrease of E-cadherin expression in HPKs (Figure 5B). Importantly, exogenous S1P exposure or SK1 overexpression did not reduce E-cadherin expression in CM cells in a cell-autonomous manner (Figures S5A and S5B). Altogether, our findings demonstrated that tumor cell-derived S1P promotes E-cadherin loss in HPKs through S1P2/3 receptor signaling but does not impair E-cadherin expression in CM cells.

E-cadherin expression is known to be regulated via several unrelated mechanisms. Whereas proteolytic processing of E-cadherin has been reported to be mainly mediated through the endocytic lysosomal and proteasomal systems or matrix metalloproteinases (MMP), repression of E-cadherin transcripts occurs via the Snail family of zinc-finger transcription factors.[24] Here, we show that the proteasome inhibitor MG132 did not inhibit S1P-induced E-cadherin downregulation, indicating that the proteasome was not involved in this process (Figure S5C). Increased expression of MMP9, but not MMP2, was observed in S1P-treated HPKs and was inhibited by JTE-013 (Figure S5D). However, the broad-spectrum MMP inhibitor batimastat[25] did not block S1P-induced E-cadherin downregulation (Figure S5E), suggesting that this effect was independent of MMPs. In contrast, analysis of transcriptional repressors of *CDH1* expression disclosed increased expression of Snail and Slug (Figures 5C and 5D), with no significant change in the expression of Zeb1/2 and Twist (Figure 5C). This upregulation was also observed in HPKs incubated with the conditioned medium from CM cells overexpressing SK1 compared with HPK grown in the conditioned medium from control cells (Figure 5E and 5F). All of these events were inhibited by S1P2 and S1P3, but not S1P1, receptor antagonists (Figures 5D and 5F). Taken together, our results suggest that E-cadherin loss in S1P-treated HPKs is mainly regulated at a transcriptional level.

The E-cadherin level is reduced in the epidermis neighboring high-SK1 tumors in reconstructed skin and patient samples

To determine whether epidermal E-cadherin expression could be an indicator of CM cell aggressiveness, HRS containing E-cadherin^{high} CM cells overexpressing or not overexpressing wild-type SK1 or SK1^{G82D} were analyzed. HRS was labeled for E-cadherin, SOX10, and nuclei by immunofluorescence multiplex staining and then processed for fluorescence microscopy. Digital image analysis of the staining allowed us to discriminate epidermis from CM cells (Figure S6A). Our results demonstrate that reduced E-cadherin expression in the epidermal compartment was linked to higher SK1 activity in the neighboring WM35 cells (Figure 6A). Similar results were obtained with G361 cells (Figure 6B), for which invasion depth into the dermis of HRS was dependent of SK1 activity (Figure S6B). These observations highlighted that the level of E-cadherin expressed in the epidermis close to tumor cells was inversely correlated with CM cell invasion into the dermis (Figure 6C). In contrast, E-cadherin expression in CM cells was not affected by SK1 activity (Figures 6A and 6B).

We next evaluated the same parameters, SK1 and E-cadherin expression and depth of invasion, in primary tumors isolated from patients with CM (Figure S6A; Table S2). Tumor specimens were separated into two groups according to SK1 expression (Figure 6D). These studies revealed that E-cadherin expression was significantly decreased in areas of the epidermis located close to primary CM expressing high levels of SK1 compared with tumors expressing low SK1 levels (Figures 6E and 6F). In contrast, E-cadherin levels in tumors were not associated with SK1 expression (Figure 6G). Importantly, our data also identified that epidermal E-cadherin expression was inversely correlated with the Breslow thickness in early-stage tumors (Figure 6H), which describes how deeply CM cells have gone into the skin.

All of these findings highlight that decreased expression of epidermal E-cadherin, associated with high SK1 expression in tumors, is correlated with the invasive potential of primary melanomas.

DISCUSSION

Most CMs arise within the epidermis before invading the dermis. Mechanisms relying on tumor cells only partially explain the early step of invasion. However, how the skin epithelium controls CM progression is still poorly understood. Keratinocytes are known to regulate melanocyte growth mainly through E-cadherin-mediated homotypic adhesion.[26] It is well accepted that the loss of keratinocyte dominance over CM cells is linked to an epithelial-mesenchymal transition (EMT)-like process, characterized by E/N-cadherin switching in CM cells.[27] However, immunohistochemistry studies did not confirm its absolute occurrence during CM progression,[5,28] and the prognostic significance of E/N-cadherin switching in CM has not been convincingly established.[5] Here, we demonstrate that the lysolipid S1P, produced by CM cells, regulates E-cadherin expression in HPKs through S1P2/3-dependent signaling, leading to Snail and Slug

(A–D) Left and center: images (scale bars, 400 μm; cell trajectories are indicated in white or red) and projections of 10 cell trajectories from one representative experiment of three with G361 (A), M249 (B), SbCl2 (C), and WM1552C (D) EGFP cells. Right: graphs reporting the motility of 40 tracked CM cells. Results are expressed in micrometers per minute; the median ± SEM is indicated.

(E and F) Graphs reporting the correlation between E-cadherin levels on CM cells and (E) the ability of HPK to inhibit CM cell motility (+HPK vs. −HPK) and (F) the paracrine impact of SK1 expression (SK1 vs. Ctrl). E-cadherin expression on CM cells was measured by flow cytometry and reported as the ratio of mean fluorescence intensity (MFI) in the presence (monoclonal antibody [mAb]) vs. absence (Ctrl) of E-cadherin antibody.

Statistical significance was determined by Kruskal-Wallis test followed by Dunn's post hoc test (A–D). (ns, not significant; ***, $p < 0.001$; ****, $p < 0.0001$) Pearson correlation coefficients and one-tailed p values are indicated (E and F).

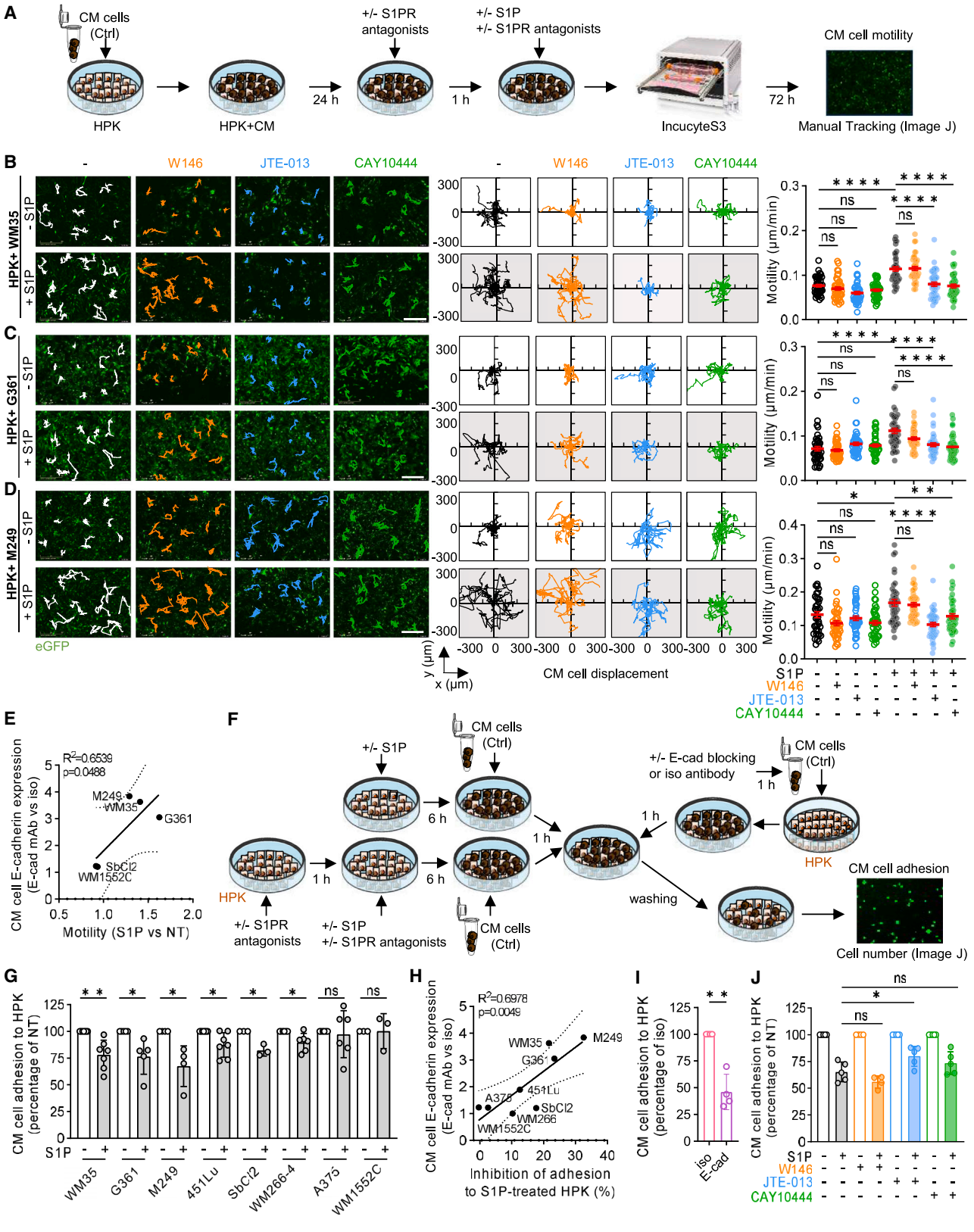

(legend on next page)

upregulation. This event subsequently promotes migration of E-cadherin-expressing CM cells, mostly by limiting their adhesion to HPKs. S1P enrichment in the tumor microenvironment could also locally modulate key events in tumor progression, such as angiogenesis/lymphangiogenesis, tumor immunity, and inflammation.[13] In addition, high levels of S1P in tumors could dictate CM cell survival by affecting the sphingolipid rheostat, thereby limiting the accumulation of its metabolic precursors, ceramide and sphingosine, known to exert pro-apoptotic effects.[29]

Recent findings have demonstrated that the protein expression profiles between nevus-associated and CM-associated keratinocytes gradually change during the transformation process.[30] Interestingly, alterations in the expression of the Par3 (PARD3) polarity protein,[31] the alarmins S100A8/A9,[32] and the cytokine thymic stromal lymphopoietin (TSLP)[33] have been detected in the keratinocyte microenvironment neighboring primary CM.

Here, we report changes in the expression of cell adhesion molecules that occurred in HPKs under the influence of melanoma S1P. Our data indicate that the tumor lipid S1P reduces the expression of E-cadherin and desmoglein-3 in HPKs. E-cadherin is critical in the control of adhesion of CM cells to keratinocytes.[34] In contrast, desmoglein-3, a desmosomal cadherin indispensable for cell-cell adhesion in keratinocytes, was never associated with the development and progression of CM but, rather, those of squamous cell carcinoma.[35]

The present study shows that S1P decreases E-cadherin expression in HPKs in an S1P2- and S1P3-dependent manner. These results are in accordance with previous studies showing S1P-induced E-cadherin downregulation mediated by S1P2 and S1P3 in alveolar epithelial cells[36] and lung fibroblasts.[37] This effect could be dependent on the Rho-family guanosine triphosphate hydrolases (GTPases)[38] as well as transforming growth factor (TGF)-β1 production, which may *trans*-activate S1P2 and S1P3.[37] However, RNA sequencing (RNA-seq) analysis did not reveal any variation in TGF-β1 expression in S1P-treated HPKs, favoring the first hypothesis.

In hepatoma cells, E-cadherin loss has been reported to be induced by intracellular S1P in SK1-overexpressing cancer cells.[39] The loss of this epithelial marker is an important step in the EMT process, and various alterations of sphingolipid metabolism, including those affecting the glycosphingolipid pattern, have been reported to regulate EMT.[40] For instance, inhibition of SK1 alters EMT-related marker expression by reducing the expression of phosphorylated focal adhesion kinase (p-FAK) in colorectal cancer cells.[41] Here, E-cadherin expression in CM cells was neither affected by SK1 overexpression nor by exogenous S1P, indicating that the SK1/S1P/S1PR pathway does not interfere with E-cadherin expression in our models. One could argue that the EMT transcription factors Snail and Slug cannot be stimulated by S1P in CM cells as they are in HPKs. Indeed, whereas *SNAI1* is not expressed in CM samples,[42,43] CM-driving extracellular signal-related kinase (ERK)-activating oncogenic pathways induce EMT transcription factor (TF) reprogramming, which is associated with downregulation of *SNAI2*.[43] Moreover, according to the phenotypic plasticity of CM cells, expression of E-cadherin is positively related to that of the microphthalmia-associated TF (MITF) and inversely related to that of N-cadherin and the AXL receptor tyrosine kinase.[44] Of note, S1P stimulates MITF expression in CM,[9] possibly affecting the state of differentiation of these cells.

The present findings establish that S1P-induced E-cadherin loss at the HPK surface is mainly regulated at a transcriptional level. Nevertheless, we observed that S1P stimulates MMP9 in HPKs in an S1P2-dependent manner. This result confirms previous studies showing that overexpression of SK1 is associated with MMP9 induction in multiple cell types,[45,46] including HPKs.[47] MMP9 has been reported to mediate epidermal growth factor (EGF)- and TGF-β1-dependent downregulation of E-cadherin in epithelial ovarian cancer

Figure 4. S1P elicits melanoma cell motility by reducing adhesion to keratinocytes through S1P2/S1P3 receptors

(A–D) Ctrl CM cell lines were co-cultured with keratinocytes (HPKs) for 24 h. Cells were then pre-treated with S1PR antagonists (W146, 10 μM; JTE-013, 2 μM; CAY10444: 10 μM) for 1 h prior to and during S1P treatment (1 μM) or left untreated. The 2D motility of EGFP-expressing CM cells (green) was monitored during 72 h by time-lapse fluorescence microscopy (Incucyte S3). Individual trajectories were manually tracked using ImageJ.

(A) Protocol.

(B–D) Left and center: images (scale bars, 400 μm; cell trajectories are indicated in white, orange, blue, or green) and projections of cell trajectories from one representative experiment of three with WM35 (B), G361 (C), and M249 (D) cells. Right: graphs reporting the motility of 40 tracked CM cells. Results are expressed in micrometers per minute; the median ± SEM is indicated.

(E) Graph reporting the correlation between E-cadherin levels on CM cells and the paracrine impact of S1P (S1P vs. not treated [NT]) on CM cell motility. E-cadherin expression on CM cells was measured by flow cytometry and reported as the ratio of MFI in the presence (mAb) vs. absence (Ctrl) of E-cadherin antibody.

(F–J) HPKs were treated with S1P (1 μM, 6 h) without or with pre-treatment with S1PR antagonists (W146, 10 μM; JTE-013, 2 μM; CAY10444, 10 μM) for 1 h prior to S1P, or CM cells were pre-treated with E-cadherin-blocking antibody. CM cells were then seeded on the HPK layer. After 1 h, CM cells adhering to HPKs after gentle washes were quantified by fluorescence microscopy.

(F) Protocols.

(G) Percentages of CM cells adhering to S1P-treated (gray) vs. vehicle-treated HPKs (NT, white).

(H) Graph reporting the correlation between E-cadherin levels on CM cells and the inhibitory effect of S1P on HPK adhesion to CM cells (percentages of CM cells adhering to S1P-treated vs. vehicle-treated HPKs). E-cadherin expression on CM cells was measured by flow cytometry and reported as the ratio of MFI in the presence (mAb) vs. absence (Ctrl) of E-cadherin antibody.

(I) Percentage of M249 cells adhering to HPKs after pre-incubation of M249 cells with an iso antibody or an E cadherin-blocking antibody (E-cad).

(J) Percentage of M249 cells adhering to S1P-treated (gray) vs. vehicle-treated HPKs (NT) in the presence or absence of S1PR antagonists. Data are from 4–7 (G), 4 (I), or 3–5 (J) independent experiments.

Statistical significance was determined by two-way ANOVA followed by Bonferroni's post-hoc test (B–D). Pearson correlation coefficients and one-tailed p values are indicated (E and H). Statistical significance was determined by paired Student's t test (G and I) or unpaired t test (J). (ns, not significant; *, $p < 0.05$; **, $p < 0.01$; ****$p < 0.0001$) See also Figure S4.

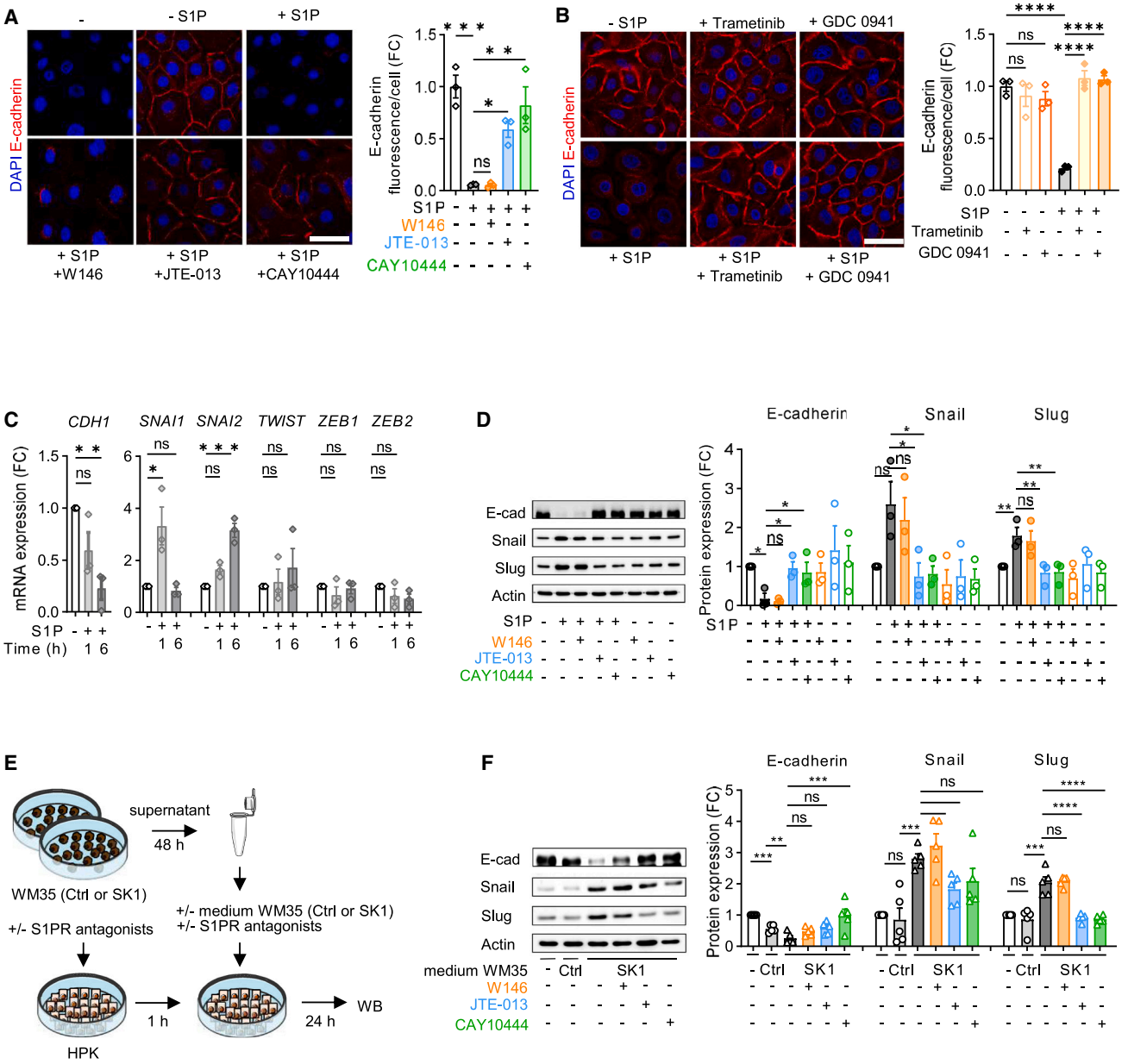

Figure 5. S1P reduces E-cadherin expression in keratinocytes through S1P2/3 signaling pathways

(A–D) HPKs were pre-treated with S1PR antagonists (W146, 10 μM; JTE-013, 2 μM; CAY10444, 10 μM), the PI3K-Akt inhibitor GDC-0941 (1 μM), or the mitogen-activated protein kinase (MAPK) inhibitor trametinib (1 μM) for 1 h prior to and during S1P treatment (1 μM for 1 h or 6 h) or left untreated.

(A and B) Left: representative confocal images of HPKs labeled for E-cadherin (red) and nuclei (DAPI) (scale bars, 50 μm). Right: E-cadherin fluorescence intensity was quantified per cell using ImageJ.

(C) mRNA levels of CDH1, SNAI1, SNAI2, TWIST, ZEB1, and ZEB2 were assessed by RT-qPCR.

(D) Left: representative western blot of E-cadherin, Snail and Slug. Right. Protein quantification was normalized to β-actin. Results are expressed in FC vs. vehicle-treated HPKs.

(E and F) HPKs were pre-treated with S1PR antagonists or left untreated before incubation with the conditioned medium (medium) from Ctrl or SK1-over-expressing WM35 cells (SK1) for 24 h.

(E) Protocol.

(F) Left: representative western blot of E-cadherin, Snail, and Slug. Right: protein quantification normalized to β-actin. Results are expressed as FC vs. HPKs incubated with the medium from Ctrl WM35 cells.

Data are mean ± SEM of 3 (A and B) or 5 (F) independent experiments. Statistical significance was determined by one-way ANOVA followed by Tukey's post hoc test (A–C) or paired one-way ANOVA followed by Dunnet's post hoc test (D and F). (ns, not significant; *, $p < 0.05$; **, $p < 0.01$; ***, $p < 0.001$; ****, $p < 0.0001$) See also Figure S5.

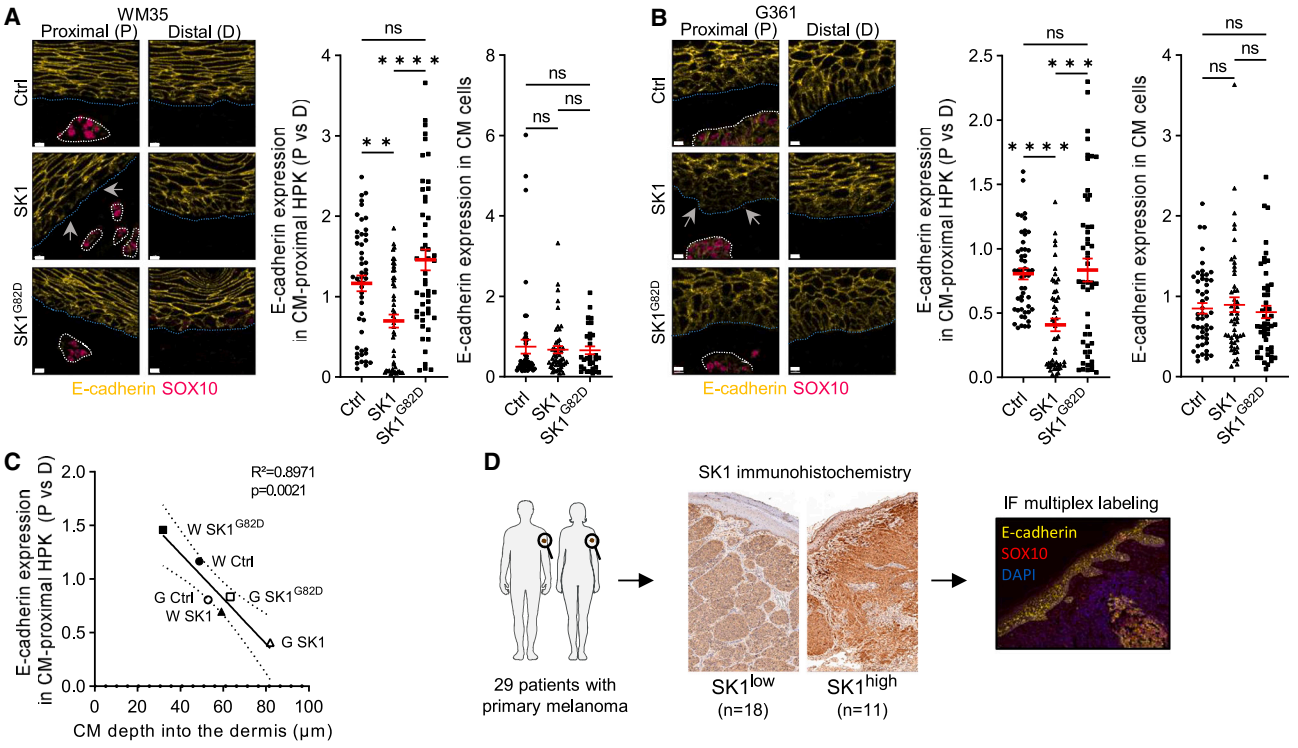

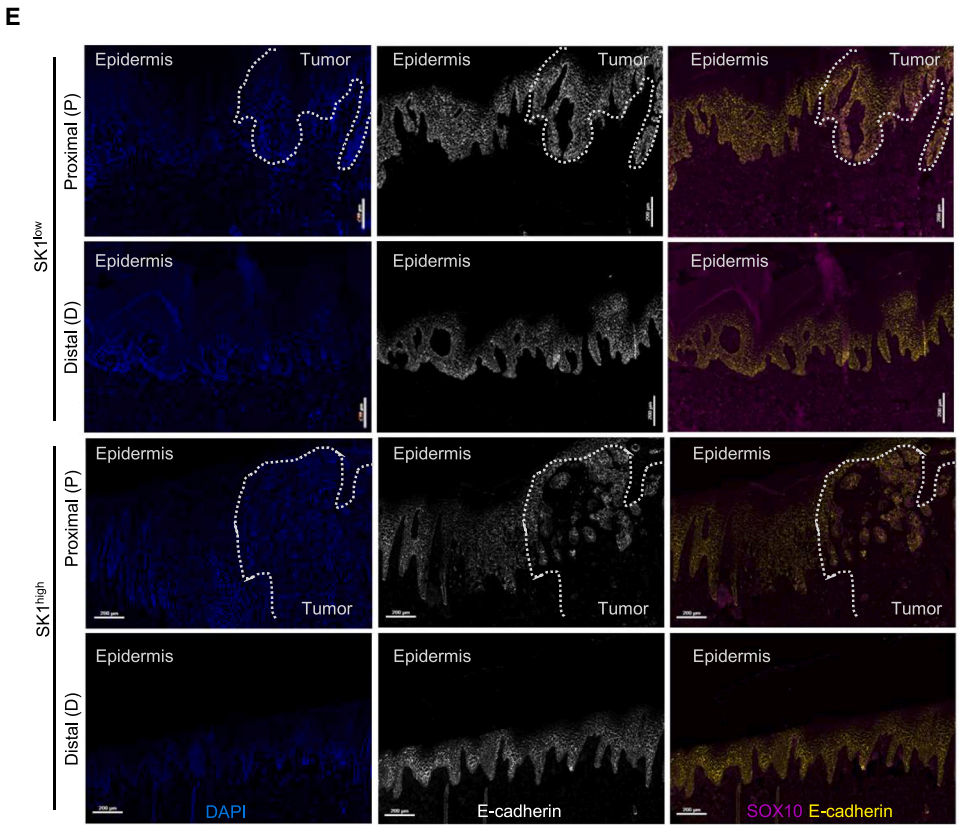

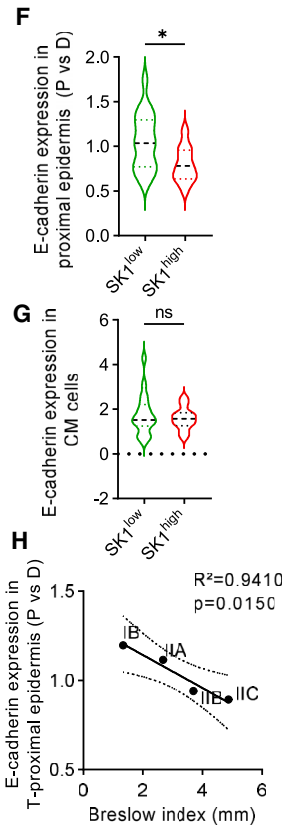

(legend on next page)

and esophageal squamous cell carcinoma,[48,49] respectively. Whereas there was no evidence of such regulation in our model, the secretion of MMP9 by keratinocytes has been reported to be dependent on the presence of CM cells and to facilitate tumor invasion into the dermis.[50] This suggests that, by producing S1P, CM cells, in addition to impairing adhesive properties, are able to stimulate the proteolytic potential of surrounding keratinocytes to invade the dermal compartment, possibly by degrading collagen IV, the major component of the basal membrane.[51]

The loss of E-cadherin induced by tumor-derived molecules may affect several functions in the human epidermis. Indeed, E-cadherin is a component of adherens junctions and mediates intercellular adhesion between keratinocytes. In this context, its loss may lead to the disruption of skin homeostasis and affect keratinocyte differentiation. As a matter of fact, as shown in nodular CM, changes in the expression pattern of the differentiation-dependent marker keratin 14 have been observed in the epidermal region surrounding the tumor site.[52] Similarly, connexins 26 and 30 are induced in the epidermis adjacent to CM compared with melanocytic nevi.[53]

Altogether, tumor S1P can reduce E-cadherin expression in epidermal keratinocytes, promoting epithelial-like CM cell motility to the dermis, mostly by limiting adhesion of keratinocytes to tumor cells. Furthermore, our findings open new avenues for (1) identifying novel and original prognostic markers to improve the metastatic risk assessment of primary CM and (2) developing new pharmacological approaches targeting SK1/S1PR2/S1PR3 as therapy adjuvants after surgery for early treatment of CM.

Limitations of the study

To identify which S1PR subtypes were involved in the cell-cell communication between keratinocytes and melanoma cells, we used S1PR antagonists. A genetic ablation approach of a given S1PR would have allowed us to overcome the off-target effects that could be induced by the chemical antagonists. However, optimizing the genetic approach has proven to be a difficult task in HPKs. Another limitation is related to the 3D integrated model of HRS that does not fully recapitulate all aspects of the tumor microenvironment, notably because it is devoid of endothelial and immune cells. However, HRS constitutes a valuable model to study the progression of primary melanoma because in humans, unlike in mice, melanomas originate from melanocytes that reside at the dermo-epidermal junction. Our findings obtained using the HRS motivate future studies using a genetically engineered mouse model in which $BRAF^{V600E}$-driven melanoma can be induced in tail interfollicular melanocytes. Interfollicular melanoma cells expand radially in the murine epidermis to form lesions that resemble human *in situ* melanomas.

STAR★METHODS

Detailed methods are provided in the online version of this paper and include the following:

- KEY RESOURCES TABLE
- RESOURCE AVAILABILITY
  - Lead contact
  - Materials availability
  - Data and code availability
- EXPERIMENTAL MODEL AND STUDY PARTICIPANT DETAILS
  - Clinical samples
  - Cell culture
  - Construction of SK1 and $SK1^{G82D}$ cell lines
  - 3D human reconstructed skin (HRS)
- METHOD DETAILS
  - Sphingolipidomic analyses
  - SK1 enzymatic assay
  - S1P secretion
  - CM cell growth
  - Immunochemistry of HRS
  - Cell motility assays
  - Wound healing assay
  - Treatments
  - RNA-sequencing
  - Flow cytometry
  - Cell adhesion assays

Figure 6. E-cadherin is reduced in epidermis neighboring high SK1 tumors and inversely correlated with melanoma invasion

(A and B) Immunofluorescence (IF) multiplex labeling of HRS sections containing WM35 (A) and G361 (B) cells overexpressing or not overexpressing (Ctrl) wild-type SK1 (SK1) or its catalytically inactive variant ($SK1^{G82D}$). Left: images of E-cadherin- and SOX10-labeled HRS regions located proximally (P) or distally (D) to CM cells (scale bar, 10 μm). Blue and white dotted lines indicate the basal lamina and the tumor cell islets, respectively. Arrows indicate epidermal areas with reduced E-cadherin expression. Center: Graphs reporting E-cadherin expression in HPKs located proximally to CM cells. Results were normalized to the mean of E-cadherin fluorescence intensity from HPKs located distantly from CM cells in the same HRS. Right: Graphs reporting E-cadherin expression in CM cells. Data are from one representative experiment of two. The median ± SEM is indicated.

(C) Graph reporting the inverse correlation between the E-cadherin expression in HPKs proximal to CM cells (W, WM35; G, G361) and the distances between CM cells and the basal lamina.

(D) Primary tumors from 29 melanoma patients were classified into 2 groups ($SK1^{low}$, n = 18; $SK1^{high}$, n = 11) according to SK1 expression assessed by immunohistochemistry (scale bar, 100 μm) and analyzed for E-cadherin and SOX-10 expression by IF multiplex labeling.

(E) Representative images of IF labeling for nuclei (DAPI, blue), E-cadherin (white or yellow), and SOX-10 (magenta) in proximal and distal epidermis from $SK1^{low}$- and $SK1^{high}$-expressing melanoma specimens. The tumor areas are indicated by a dotted line (scale bar, 200 μm).

(F and G) Graphs reporting E-cadherin expression in tumor-proximal epidermis normalized to tumor-distal epidermis (F) and in tumors (G). The median ± SEM is indicated.

(H) Graph reporting the inverse correlation between E-cadherin expression in tumor-proximal epidermis normalized to tumor-distal epidermis and the mean of the Breslow index in the early stages; IB (n = 5), IIA (n = 5), IIB (n = 7), and IIC (n = 4).

Statistical significance was determined by Kruskal-Wallis test followed by Dunn's post hoc test (A and B), by Student's t test (F), and Mann-Whitney test (G). (ns, not significant; *, $p < 0.05$; **, $p < 0.01$; ***, $p < 0.001$; ****, $p < 0.0001$) Pearson correlation coefficient and one-tailed p value are indicated (C and H). See also Figure S6 and Table S2.

- Immunofluorescence staining of 2D samples
- Quantitative RT-PCR
- Western blot analyses
- Preparation of conditioned medium
- Quantification of MMP secretion by zymography
- Immunohistochemistry of melanomas
- Immunofluorescence of HRS and melanomas

- QUANTIFICATION AND STATISTICAL ANALYSIS

SUPPLEMENTAL INFORMATION

Supplemental information can be found online at https://doi.org/10.1016/j.celrep.2023.113586.

ACKNOWLEDGMENTS

Financial support by INSERM, Paul Sabatier University, Institut National du Cancer, Fondation ARC, and the Société Française de Dermatologie is gratefully acknowledged. The research leading to these results has received funding from the Transcan-2 Research Program, which is a transnational R&D program jointly funded by national funding organizations within the framework of the ERA-NET Transcan-2. J.N. is a recipient of a fellowship from Fondation ARC. L.C. is a recipient of fellowships from Fondation pour la Recherche Médicale (ECO201906008956) and Fondation ARC (ARCDOC42022010004548). This study was partially supported through the grant EUR CARe ANR-18-EURE-0003 in the framework of the Programme des Investissements d'Avenir. We thank the CARe graduate school for support for M.G.. We thank the staff of the histology (Anexplo platform, CRB, and Ibisa, Toulouse, France), cell imaging, vectorology, and transcriptomics (INSERM UMR1037, Toulouse, France) facilities. We are grateful for the use of the Imag'IN Platform of the Institut Universitaire du Cancer Toulouse-Oncopole (www.imagin-labs.net/imagin_v2). Incucyte technology was rendered accessible thanks to financial support from ITMO Cancer of Aviesan within the framework of the 2021–2030 Cancer Control Strategy with funds administered by INSERM. The help of Genoskin (Toulouse, France) and the Toulouse Children's Hospital (CIC1436, Pediatric Unit, CHU Toulouse, Profs. P. Galinier and O. Abbo and Dr. F. Auriol) for providing skin samples is also acknowledged. This work was granted access to the HPC resources of the CALMIP supercomputing center under allocation 2019-T19001. We are grateful to the Genotoul Bioinformatics Platform Toulouse Midi-Pyrénées for providing computing resources. We also thank Drs. Josefina Casas and Gemma Fabriàs (Institute of Advanced Chemistry of Catalonia—Spanish Council for Scientific Research: Barcelona, Catalonia, Spain) for sphingolipid measurements. We thank Drs. Anne Montfort, Céline Colacios, Marie-Pierre Rols, and Elie Marcheteau for technical support, scientific discussions, and critical reading of the manuscript. The graphical abstract was created with BioRender.

AUTHOR CONTRIBUTIONS

Conceptualization, J.N., L.C., J.R., and N.A.-A.; methodology, J.N., L.C., V.G., A.S., and L.G.; software, M. Grimont and M. Genais; formal analysis, L.C., M. Grimont, and M. Genais; investigation, J.N., L.C., V.G., M. Grimont, A.S., E.M., S.C., and J.C.; resources, A.E., T.L., S.P., T.T., J.M., O.H., J.L., S.D., and J.C.; writing—review and editing, J.N., L.C., M. Grimont, A.E., B.S., L.N., T.L., J.C., L.G., J.R., and N.A.-A; supervision, J.R. and N.A.-A.; funding acquisition, J.R. and N.A.-A.

DECLARATION OF INTERESTS

The authors declare no competing interests.

Received: June 8, 2023
Revised: October 20, 2023
Accepted: November 30, 2023
Published: December 18, 2023

REFERENCES

1. Shain, A.H., and Bastian, B.C. (2016). From melanocytes to melanomas. Nat. Rev. Cancer *16*, 345–358.
2. Wolchok, J.D., Chiarion-Sileni, V., Gonzalez, R., Grob, J.J., Rutkowski, P., Lao, C.D., Cowey, C.L., Schadendorf, D., Wagstaff, J., Dummer, R., et al. (2022). Long-Term Outcomes With Nivolumab Plus Ipilimumab or Nivolumab Alone Versus Ipilimumab in Patients With Advanced Melanoma. J. Clin. Oncol. *40*, 127–137.
3. Belter, B., Haase-Kohn, C., and Pietzsch, J. (2017). Biomarkers in Malignant Melanoma: Recent Trends and Critical Perspective. In Cutaneous Melanoma: Etiology and Therapy, W.H. Ward and J.M. Farma, eds. (Codon Publications).
4. Danen, E.H., de Vries, T.J., Morandini, R., Ghanem, G.G., Ruiter, D.J., and van Muijen, G.N. (1996). E-cadherin expression in human melanoma. Melanoma Res. *6*, 127–131.
5. Yan, S., Holderness, B.M., Li, Z., Seidel, G.D., Gui, J., Fisher, J.L., and Ernstoff, M.S. (2016). Epithelial-Mesenchymal Expression Phenotype of Primary Melanoma and Matched Metastases and Relationship with Overall Survival. Anticancer Res. *36*, 6449–6456.
6. Haroon, A., Shafi, S., and Rao, B.K. (2017). Using Reflectance Confocal Microscopy in Skin Cancer Diagnosis. Dermatol. Clin. *35*, 457–464.
7. Corbalán-Vélez, R., Oviedo-Ramírez, I., Martínez-Barba, E., and Clemente-Ruiz de Almirón, A. (2011). Epidermal effacement in malignant melanoma. Actas Dermosifiliogr. *102*, 634–635.
8. Albinet, V., Bats, M.L., Huwiler, A., Rochaix, P., Chevreau, C., Ségui, B., Levade, T., and Andrieu-Abadie, N. (2014). Dual role of sphingosine kinase-1 in promoting the differentiation of dermal fibroblasts and the dissemination of melanoma cells. Oncogene *33*, 3364–3373.
9. Garandeau, D., Noujarède, J., Leclerc, J., Imbert, C., Garcia, V., Bats, M.L., Rambow, F., Gilhodes, J., Filleron, T., Meyer, N., et al. (2019). Targeting the Sphingosine 1-Phosphate Axis Exerts Potent Antitumor Activity in BRAFi-Resistant Melanomas. Mol. Cancer Ther. *18*, 289–300.
10. Leclerc, J., Garandeau, D., Pandiani, C., Gaudel, C., Bille, K., Nottet, N., Garcia, V., Colosetti, P., Pagnotta, S., Bahadoran, P., et al. (2019). Lysosomal acid ceramidase ASAH1 controls the transition between invasive and proliferative phenotype in melanoma cells. Oncogene *38*, 1282–1295.
11. Imbert, C., Montfort, A., Fraisse, M., Marcheteau, E., Gilhodes, J., Martin, E., Bertrand, F., Marcellin, M., Burlet-Schiltz, O., Peredo, A.G.d., et al. (2020). Resistance of melanoma to immune checkpoint inhibitors is overcome by targeting the sphingosine kinase-1. Nat. Commun. *11*, 437–514.
12. Heffernan-Stroud, L.A., and Obeid, L.M. (2013). Sphingosine kinase 1 in cancer. Adv. Cancer Res. *117*, 201–235.
13. Ogretmen, B. (2018). Sphingolipid metabolism in cancer signalling and therapy. Nat. Rev. Cancer *18*, 33–50.
14. Borodzicz, S., Rudnicka, L., Mirowska-Guzel, D., and Cudnoch-Jedrzejewska, A. (2016). The role of epidermal sphingolipids in dermatologic diseases. Lipids Health Dis. *15*, 13.
15. Allende, M.L., Sipe, L.M., Tuymetova, G., Wilson-Henjum, K.L., Chen, W., and Proia, R.L. (2013). Sphingosine-1-phosphate phosphatase 1 regulates keratinocyte differentiation and epidermal homeostasis. J. Biol. Chem. *288*, 18381–18391.
16. Kunz, M., Löffler-Wirth, H., Dannemann, M., Willscher, E., Doose, G., Kelso, J., Kottek, T., Nickel, B., Hopp, L., Landsberg, J., et al. (2018). RNA-seq analysis identifies different transcriptomic types and developmental trajectories of primary melanomas. Oncogene *37*, 6136–6151.
17. Kawahara, A., Nishi, T., Hisano, Y., Fukui, H., Yamaguchi, A., and Mochizuki, N. (2009). The sphingolipid transporter spns2 functions in migration of zebrafish myocardial precursors. Science *323*, 524–527.
18. Mitra, P., Oskeritzian, C.A., Payne, S.G., Beaven, M.A., Milstien, S., and Spiegel, S. (2006). Role of ABCC1 in export of sphingosine-1-phosphate from mast cells. Proc. Natl. Acad. Sci. USA *103*, 16394–16399.

19. Takabe, K., Kim, R.H., Allegood, J.C., Mitra, P., Ramachandran, S., Nagahashi, M., Harikumar, K.B., Hait, N.C., Milstien, S., and Spiegel, S. (2010). Estradiol induces export of sphingosine 1-phosphate from breast cancer cells via ABCC1 and ABCG2. J. Biol. Chem. *285*, 10477–10486.

20. Athanasiou, K.A., Eswaramoorthy, R., Hadidi, P., and Hu, J.C. (2013). Self-organization and the self-assembling process in tissue engineering. Annu. Rev. Biomed. Eng. *15*, 115–136.

21. D'Arcy, C., and Kiel, C. (2021). Cell Adhesion Molecules in Normal Skin and Melanoma. Biomolecules *11*, 1213.

22. Krengel, S., Grotelüschen, F., Bartsch, S., and Tronnier, M. (2004). Cadherin expression pattern in melanocytic tumors more likely depends on the melanocyte environment than on tumor cell progression. J. Cutan. Pathol. *31*, 1–7.

23. Brinkmann, V. (2007). Sphingosine 1-phosphate receptors in health and disease: mechanistic insights from gene deletion studies and reverse pharmacology. Pharmacol. Ther. *115*, 84–105.

24. van Roy, F., and Berx, G. (2008). The cell-cell adhesion molecule E-cadherin. Cell. Mol. Life Sci. *65*, 3756–3788.

25. Rasmussen, H.S., and McCann, P.P. (1997). Matrix metalloproteinase inhibition as a novel anticancer strategy: a review with special focus on batimastat and marimastat. Pharmacol. Ther. *75*, 69–75.

26. Haass, N.K., Smalley, K.S.M., Li, L., and Herlyn, M. (2005). Adhesion, migration and communication in melanocytes and melanoma. Pigment Cell Res. *18*, 150–159.

27. Kuphal, S., and Bosserhoff, A.K. (2012). E-cadherin cell-cell communication in melanogenesis and during development of malignant melanoma. Arch. Biochem. Biophys. *524*, 43–47.

28. Murtas, D., Maxia, C., Diana, A., Pilloni, L., Corda, C., Minerba, L., Tomei, S., Piras, F., Ferreli, C., and Perra, M.T. (2017). Role of epithelial-mesenchymal transition involved molecules in the progression of cutaneous melanoma. Histochem. Cell Biol. *148*, 639–649.

29. Newton, J., Lima, S., Maceyka, M., and Spiegel, S. (2015). Revisiting the sphingolipid rheostat: Evolving concepts in cancer therapy. Exp. Cell Res. *333*, 195–200.

30. Ostalecki, C., Lee, J.H., Dindorf, J., Collenburg, L., Schierer, S., Simon, B., Schliep, S., Kremmer, E., Schuler, G., and Baur, A.S. (2017). Multiepitope tissue analysis reveals SPPL3-mediated ADAM10 activation as a key step in the transformation of melanocytes. Sci. Signal. *10*, eaai8288.

31. Mescher, M., Jeong, P., Knapp, S.K., Rübsam, M., Saynisch, M., Kranen, M., Landsberg, J., Schlaak, M., Mauch, C., Tüting, T., et al. (2017). The epidermal polarity protein Par3 is a non-cell autonomous suppressor of malignant melanoma. J. Exp. Med. *214*, 339–358.

32. Kiuru, M., Kriner, M.A., Wong, S., Zhu, G., Terrell, J.R., Li, Q., Hoang, M., Beechem, J., and McPherson, J.D. (2022). High-Plex Spatial RNA Profiling Reveals Cell Type–Specific Biomarker Expression during Melanoma Development. J. Invest. Dermatol. *142*, 1401–1412.e20.

33. Yao, W., German, B., Chraa, D., Braud, A., Hugel, C., Meyer, P., Davidson, G., Laurette, P., Mengus, G., Flatter, E., et al. (2022). Keratinocyte-derived cytokine TSLP promotes growth and metastasis of melanoma by regulating the tumor-associated immune microenvironment. JCI Insight *7*, e161438.

34. Li, G., Satyamoorthy, K., and Herlyn, M. (2002). Dynamics of cell interactions and communications during melanoma development. Crit. Rev. Oral Biol. Med. *13*, 62–70.

35. Hoque Apu, E., Akram, S.U., Rissanen, J., Wan, H., and Salo, T. (2018). Desmoglein 3 - Influence on oral carcinoma cell migration and invasion. Exp. Cell Res. *370*, 353–364.

36. Milara, J., Navarro, R., Juan, G., Peiró, T., Serrano, A., Ramón, M., Morcillo, E., and Cortijo, J. (2012). Sphingosine-1-phosphate is increased in patients with idiopathic pulmonary fibrosis and mediates epithelial to mesenchymal transition. Thorax *67*, 147–156.

37. Kono, Y., Nishiuma, T., Nishimura, Y., Kotani, Y., Okada, T., Nakamura, S.I., and Yokoyama, M. (2007). Sphingosine kinase 1 regulates differentiation of human and mouse lung fibroblasts mediated by TGF-beta1. Am. J. Respir. Cell Mol. Biol. *37*, 395–404.

38. Blaho, V.A., and Hla, T. (2014). An update on the biology of sphingosine 1-phosphate receptors. J. Lipid Res. *55*, 1596–1608.

39. Liu, H., Ma, Y., He, H.W., Zhao, W.L., and Shao, R.G. (2017). SPHK1 (sphingosine kinase 1) induces epithelial-mesenchymal transition by promoting the autophagy-linked lysosomal degradation of CDH1/E-cadherin in hepatoma cells. Autophagy *13*, 900–913.

40. Levade, T., Andrieu-Abadie, N., Micheau, O., Legembre, P., and Ségui, B. (2015). Sphingolipids modulate the epithelial-mesenchymal transition in cancer. Cell Death Discov. *1*, 15001.

41. Xu, C.Y., Liu, S.Q., Qin, M.B., Zhuge, C.F., Qin, L., Qin, N., Lai, M.Y., and Huang, J.A. (2017). SphK1 modulates cell migration and EMT-related marker expression by regulating the expression of p-FAK in colorectal cancer cells. Int. J. Mol. Med. *39*, 1277–1284.

42. Mikesh, L.M., Kumar, M., Erdag, G., Hogan, K.T., Molhoek, K.R., Mayo, M.W., and Slingluff, C.L., Jr. (2010). Evaluation of molecular markers of mesenchymal phenotype in melanoma. Melanoma Res. *20*, 485–495.

43. Caramel, J., Papadogeorgakis, E., Hill, L., Browne, G.J., Richard, G., Wierinckx, A., Saldanha, G., Osborne, J., Hutchinson, P., Tse, G., et al. (2013). A switch in the expression of embryonic EMT-inducers drives the development of malignant melanoma. Cancer Cell *24*, 466–480.

44. Kim, J.E., Leung, E., Baguley, B.C., and Finlay, G.J. (2013). Heterogeneity of expression of epithelial-mesenchymal transition markers in melanocytes and melanoma cell lines. Front. Genet. *4*, 97.

45. Tamashiro, P.M., Furuya, H., Shimizu, Y., and Kawamori, T. (2014). Sphingosine kinase 1 mediates head & neck squamous cell carcinoma invasion through sphingosine 1-phosphate receptor 1. Cancer Cell Int. *14*, 76.

46. Liu, S.Q., Xu, C.Y., Wu, W.H., Fu, Z.H., He, S.W., Qin, M.B., and Huang, J.A. (2019). Sphingosine kinase 1 promotes the metastasis of colorectal cancer by inducing the epithelialmesenchymal transition mediated by the FAK/AKT/MMPs axis. Int. J. Oncol. *54*, 41–52.

47. Shin, K.O., Choe, S.J., Uchida, Y., Kim, I., Jeong, Y., and Park, K. (2018). Ginsenoside Rb1 Enhances Keratinocyte Migration by a Sphingosine-1-Phosphate-Dependent Mechanism. J. Med. Food *21*, 1129–1136.

48. Cowden Dahl, K.D., Symowicz, J., Ning, Y., Gutierrez, E., Fishman, D.A., Adley, B.P., Stack, M.S., and Hudson, L.G. (2008). Matrix metalloproteinase 9 is a mediator of epidermal growth factor-dependent e-cadherin loss in ovarian carcinoma cells. Cancer Res. *68*, 4606–4613.

49. Bai, X., Li, Y.Y., Zhang, H.Y., Wang, F., He, H.L., Yao, J.C., Liu, L., and Li, S.S. (2017). Role of matrix metalloproteinase-9 in transforming growth factor-beta1-induced epithelial-mesenchymal transition in esophageal squamous cell carcinoma. OncoTargets Ther. *10*, 2837–2847.

50. Van Kilsdonk, J.W.J., Bergers, M., Van Kempen, L.C.L.T., Schalkwijk, J., and Swart, G.W.M. (2010). Keratinocytes drive melanoma invasion in a reconstructed skin model. Melanoma Res. *20*, 372–380.

51. Hofmann, U.B., Westphal, J.R., Van Muijen, G.N., and Ruiter, D.J. (2000). Matrix metalloproteinases in human melanoma. J. Invest. Dermatol. *115*, 337–344.

52. Kodet, O., Lacina, L., Krejčí, E., Dvořánková, B., Grim, M., Štork, J., Kodetová, D., Vlček, Č., Šáchová, J., Kolář, M., et al. (2015). Melanoma cells influence the differentiation pattern of human epidermal keratinocytes. Mol. Cancer *14*, 1.

53. Haass, N.K., Ripperger, D., Wladykowski, E., Dawson, P., Gimotty, P.A., Blome, C., Fischer, F., Schmage, P., Moll, I., and Brandner, J.M. (2010). Melanoma progression exhibits a significant impact on connexin expression patterns in the epidermal tumor microenvironment. Histochem. Cell Biol. *133*, 113–124.

54. Sirven, A., Ravet, E., Charneau, P., Zennou, V., Coulombel, L., Guétard, D., Pflumio, F., and Dubart-Kupperschmitt, A. (2001). Enhanced transgene expression in cord blood CD34(+)-derived hematopoietic cells, including

developing T cells and NOD/SCID mouse repopulating cells, following transduction with modified trip lentiviral vectors. Mol. Ther. *3*, 438–448.

55. Gibot, L., Galbraith, T., Bourland, J., Rogic, A., Skobe, M., and Auger, F.A. (2017). Tissue-engineered 3D human lymphatic microvascular network for in vitro studies of lymphangiogenesis. Nat. Protoc. *12*, 1077–1088.
56. Gibot, L., Galbraith, T., Huot, J., and Auger, F.A. (2013). Development of a tridimensional microvascularized human skin substitute to study melanoma biology. Clin. Exp. Metastasis *30*, 83–90.
57. Cingolani, F., Casasampere, M., Sanllehí, P., Casas, J., Bujons, J., and Fabrias, G. (2014). Inhibition of dihydroceramide desaturase activity by the sphingosine kinase inhibitor SKI II. J. Lipid Res. *55*, 1711–1720.
58. Mitra, P., Payne, S.G., Milstien, S., and Spiegel, S. (2007). A rapid and sensitive method to measure secretion of sphingosine-1-phosphate. Methods Enzymol. *434*, 257–264.
59. Love, M.I., Huber, W., and Anders, S. (2014). Moderated estimation of fold change and dispersion for RNA-seq data with DESeq2. Genome Biol. *15*, 550.
60. Gu, Z., Eils, R., and Schlesner, M. (2016). Complex heatmaps reveal patterns and correlations in multidimensional genomic data. Bioinformatics *32*, 2847–2849.
61. Wickham, H. (2016). ggplot2 (Springer Cham).

STAR★METHODS

KEY RESOURCES TABLE

REAGENT or RESOURCE	SOURCE	IDENTIFIER
Antibodies		
Mouse monoclonal anti-human Tyrosinase (T311)	Agilent	Cat# M3623; RRID: AB_2210866
Rabbit polyclonal anti-human SPHK1	Abcam	Cat# ab260073; discontinued
Mouse monoclonal anti-human E-cadherin (SHE78-7)	Thermo Fischer Scientific	Cat# 13–5700; RRID: AB_2533022
Rabbit monoclonal anti-human E-Cadherin (EP700Y)	Abcam.	Cat# ab40772; RRID: AB_731493
Rabbit monoclonal anti-human E-cadherin (24E10)	Cell Signaling Technology	Cat# 3195S; RRID: AB_2291471
Mouse monoclonal anti-human E-cadherin (clone 36)	Ventana	Cat# 790–4497; antibody for *in vitro* diagnostic use
Goat anti-rabbit IgG, Alexa Fluor 647	Invitrogen	Cat# 32733; RRID: AB_2633282
Goat anti-rabbit IgG, Alexa Fluor 546	Invitrogen	Cat# A11010; RRID: AB_2534077
Mouse monoclonal anti-human SOX10 (A-2)	Santa Cruz	Cat# sc-365692; RRID: AB_10844002
Rabbit monoclonal anti-human Snail (C15D3)	Cell Signaling Technology	Cat# 3879S; RRID: AB_2255011
Rabbit monoclonal anti-human Slug (C19G7)	Cell Signaling Technology	Cat# 9585S; RRID: AB_2239535)
Rabbit monoclonal anti-human β-Actin (13E5)	Cell Signaling Technology	Cat #4970; RRID: AB_2223172
Anti-Rabbit IgG, HRP linked Ab	Cell Signaling Technology	Cat#7074; RRID: AB_2099233
Biological samples		
Adult skin biopsies obtained from abdominal reductive surgeries	Genoskin (Toulouse, France)	Permit AC-2011-1443 from the French Ministry of Higher Education and Research
Young patients' foreskins	Children Hospital (Toulouse, France).	Contract 17092C
Plasma samples from melanoma patients and healthy individuals	Biobank of Hospital Clínic - IDIBAPS (Barcelona, Spain)	Code: R120904-090; National Registry: Code: ISCIII C.0000334
Primary melanoma FFPE tumor samples	Biological Resource Center of the Lyon Sud Hospital (Hospices civils de Lyon, France)	Registration number: n°22_5837
Chemicals, peptides, and recombinant proteins		
Dispase II	Sigma-Aldrich	Cat# D4693
Dermalife K medium	Cellsystems	Cat# LL-0007
Collagenase H	Sigma-Aldrich	Cat# 11074032001
MCDB153 medium	Sigma-Aldrich	Cat# M7403
Leibovitz's L-15 medium	Thermo Fisher Scientific	Cat# 11415064
Ham's F-12 medium	Thermo Fisher Scientific	Cat# N4888
Dulbecco's Modified Eagle Medium (DMEM)	Thermo Fisher Scientific	Cat# 61965026
Roswell Park Memorial Institute (RPMI)	Thermo Fisher Scientific	Cat# 61870044
Human Insulin	Sigma-Aldrich	Cat# i9278
Ascorbic acid	Sigma-Aldrich	Cat# A4034
Hydroxycortisone	Sigma-Aldrich	Cat# H0888
Bovine insulin	Sigma-Aldrich	Cat# i6634
Cholera toxin from Vibrio cholerae	Sigma-Aldrich	Cat# C8052

(*Continued on next page*)

Continued

REAGENT or RESOURCE	SOURCE	IDENTIFIER
ATP	Sigma-Aldrich	Cat# FLAAS
[y-32P]ATP	Perkin-Elmer	Cat# BLU502Z
D-*erythro*-Sphingosine	Biomol	Cat# MTY-1802
D-*erythro*-[3-^{3}H]sphingosine	Isobio	Cat# ART-0490
S1PR antagonist W146	Sigma-Aldrich	Cat# W1020
S1PR antagonist JTE-013	Sigma-Aldrich	Cat# J4080
S1PR antagonist CAY10444	Cayman Chemicals	Cat# 10005033
proteasome inhibitor MG132	Selleckchem	Cat# S2619
MMP inhibitor Batimastat	Sigma-Aldrich	Cat# SML0041
MEK inhibitor Trametinib	MedChemExpress	Cat# HY-10999A
PI3K inhibitor GDC 0941	Axon Medchem	Cat# 1377
Target Retrieval solution High pH (pH 8)	Agilent	Cat# K8004
Critical commercial assays		
Envision HRP secondary detection system using DAB	Agilent	Cat# 5007
Hematoxylin Link	Agilent	Cat# K800821
RNeasy Plus Mini Kit	Qiagen	Cat# 74134
Truseq Stranded mRNA library prep	Illumina	Cat# 20020594
IDT for Illumina Truseq RNA UD Indexes	Illumina	Cat# 20022371
NextSeq 550 High Output Kit v2.5	Illumina	Cat# 20024907
KAPA Library Quantification Kit Illumina platforms	KapaBiosystems	Cat# KK4824
HS NGS Fragment Kit	Agilent	Cat# DNF-474-0500
Quant-iT RNA assay kit, Broad range	Invitrogen	Cat# Q10213
Opal 6-Plex Manual Detection Kit	Akoya Biosciences	Cat# SKU NEL811001KT
BOND Epitope Retrieval Solution 2 (EDTA, pH9)	Leica Biosystems	Cat# AR9640
Deposited data		
Code for analyzing and representing RNA sequencing	This paper	https://doi.org/10.5281/zenodo.10142336
RNA-seq data files along with their associated metadata	This paper	GSE230050
Gene expression data from nevi and tumors	Kunz et al.[16]	GSE11250915
Gene expression and clinical data of Skin Cutaneous Melanoma dataset	The Cancer Genome Atlas (TCGA)	http://www.genome.ucsc.edu/
Unprocessed Western blots - Figures 5D-5F-S5C-S5D-S5E	This paper	https://doi.org/10.17632/4bzwh68gb3.1
Experimental models: Cell lines		
WM35 cells	Dr. M. Herlyn (The Wistar Institute, Philadelphia, PA)	RRID:CVCL_0580; female
Ctrl WM35 cells	This manuscript	N/A
SK1 WM35 cells	This manuscript	N/A
SK1^{G82D} WM35 cells	This manuscript	N/A
G361 cells	ATCC (LGC)	RRID:CVCL_1220; male
Ctrl G361 cells	This manuscript	N/A
SK1 G361 cells	This manuscript	N/A
SK1^{G82D} G361 cells	This manuscript	N/A
M249	Dr. R.S. Lo (University of California, Los Angeles, CA).	RRID:CVCL_D755; sex unspecified

(*Continued on next page*)

Continued

REAGENT or RESOURCE	SOURCE	IDENTIFIER
SbCl2 cells	Dr. S. Tartare-Deckert (Université Nice Sophia-Antipolis, Inserm, Center Méditerranéen de Médecine Moléculaire, Nice, France)	RRID:CVCL_D732; male
WM1552C	Rockland Immunochemicals, Inc	RRID:CVCL_6472; male
451Lu cells	Dr. S. Tartare-Deckert (Université Nice Sophia-Antipolis, Inserm, Center Méditerranéen de Médecine Moléculaire, Nice, France)	RRID:CVCL_6357; male
WM266-4	ATCC (LGC)	RRID:CVCL_2765; female
A375	ATCC (LGC)	RRID:CVCL_0132; female
Oligonucleotides		
CDH1	QuantiTect, Qiagen	QT00080143
SNAI1	QuantiTect, Qiagen	QT00010010
SNAI2	QuantiTect, Qiagen	QT00044128
TWIST1	QuantiTect, Qiagen	QT00011956
ZEB1	QuantiTect, Qiagen	QT00020972
ZEB2	QuantiTect, Qiagen	QT00008554
GAPDH	QuantiTect, Qiagen	QT00079247
ACTB	QuantiTect, Qiagen	QT00095431
Software and algorithms		
R 4.1.2	R Foundation for Statistical Computing	https://www.npackd.org/p/r/4.1.2
R Bioconductor package DESeq2 v1.38	Bioconductor	https://bioconductor.org/packages/release/bioc/html/DESeq2.html
fgsea R-package	Bioconductor	https://bioconductor.org/packages/release/bioc/html/fgsea.html
StepOne v 2.3–5	Applied Biosystems	https://www.thermofisher.com/fr/fr/home/technical-resources/software-downloads/StepOne-and-StepOnePlus-Real-Time-PCR-System.html
CaseViewer v2.4.0.1190028–1	3DHISTECH Ltd	https://www.3dhistech.com/research/software-downloads/
IncuCyte Cell-by-Cell Analysis software module v 2020b (20202.1.7501.19684–1)	Sartorius	https://www.sartorius.com/en/products/live-cell-imaging-analysis/live-cell-analysis-software/incucyte-cell-by-cell-analysis-software?utm_source=google&utm_medium=cpc&utm_campaign=incucyte&utm_term=brand&utm_content=search&gad_source=1&gclid=EAIaIQobChMI_7iVwbDcggMVk0FBAh0cNQ8-EAAYASAAEgL9zPD_BwE
Harmony high-content imaging and analysis v4.9	Perkin Elmer	https://www.perkinelmer.com/fr/product/harmony-4-9-office-license-hh17000010
ImageJ v 1.52p	ImageJ	https://github.com/ImageJ
ImageJ plugin "Manual tracking"	F. Cordelières, Institut Curie (Orsay, France)	https://ImageJ.net/ij/plugins/track/track.html
Imaris version 9.9.1	Oxford Instruments	https://imaris.oxinst.com/
Image Lab v 6.1	Bio-Rad	https://www.bio-rad.com/fr-fr/product/image-lab-software?ID=KRE6P5E8Z

(*Continued on next page*)

Continued

REAGENT or RESOURCE	SOURCE	IDENTIFIER
inForm Advanced Analysis Software v 2.6.0	Akoya Biosciences	https://www.akoyabio.com/support/software/
Phenochart Whole Slide Viewer	Perkin Elmer	https://www.perkinelmer.com.cn/lab-products-and-services/resources/tissue-imaging-software-downloads.html
GraphPad Prism v 9.5.0	GraphPad Software Inc	https://www.graphpad.com/features
BD FACSDiva v9.0.1 software	BD Biosciences	https://www.bdbiosciences.com/en-us/products/software/instrument-software/bd-facsdiva-software
FlowJo™ v10.8.1 software		https://www.flowjo.com/solutions/flowjo/downloads/previous-versions
Other		
IncuCyte® S3 Live-Cell system	Sartorius	https://www.sartorius.com/en/products/live-cell-imaging-analysis/live-cell-analysis-instruments/s3-live-cell-analysis-instrument
Illumina NextSeq 550 instrument	Illumina	https://www.illumina.com/systems/sequencing-platforms/nextseq.html

RESOURCE AVAILABILITY

Lead contact

Further information and requests for resources and reagents should be directed to and will be fulfilled by the lead contact: Nathalie Andrieu-Abadie (nathalie.andrieu@inserm.fr).

Materials availability

Cell lines generated in this study are available on reasonable request.

Data and code availability

RNA-seq data files along with their associated metadata have been deposited in the GEO database under the accession code GSE230050 and are publicly available as of the date of publication. Gene expression data from nevi and tumors (GEO DataSets: GSE112509 [16]) were downloaded from NCBI and analyzed by GraphPad Prism 9. Gene expression and clinical data of The Cancer Genome Atlas (TCGA) Skin Cutaneous Melanoma dataset were downloaded from the UCSC cancer genome browser project (http://www.genome.ucsc.edu/) and analyzed by GraphPad Prism 9. Accession numbers are listed in the key resources table.

Microscopy data reported in this paper will be shared by the lead contact upon request.

(1) Custom scripts are available at https://github.com/gepmat/S1P_keratinocytes (doi.org/10.5281/zenodo.10142336) and are publicly available as of the date of publication. The link is also listed in the key resources table.

Interactive plots linking scores to cell localization were developed using the R package Shiny from Chang, W., Cheng, J., Allaire, J., Sievert, C., Schloerke, B., Xie, Y., Allen, J., McPherson, J., Dipert, A. & Borges, B. (2023). Shiny: Web Application Framework for R. R package version 1.7.4.9002, https://shiny.rstudio.com/

(1) Unprocessed Western blots from Figures 5D-5F-S5C-S5D-S5E were deposited on Mendeley data: https://doi.org/10.17632/4bzwh68gb3.1
(2) Any additional information required to reanalyze the data reported in this paper is available from the lead contact upon request.

EXPERIMENTAL MODEL AND STUDY PARTICIPANT DETAILS

Clinical samples

(1) Plasma samples from 10 healthy individuals and 5 primary melanoma patients were obtained from the collection at the Biobank of the Melanoma Unit of the Hospital Clinic of Barcelona (HCB, Spain). The "Colección de la Unitat de melanoma" is registered at the Biobank of Hospital Clínic-IDIBAPS (Code R120904-090) and at the National Registry (Code ISCIII C.0000334).

Primary melanoma FFPE tumor samples were obtained through the Biological Resource Center of the Lyon Sud Hospital (Hospices civils de Lyon, France). The selected 29 cutaneous tumor biopsies, including adjacent epidermis, were collected before any treatment.

Patient clinical information is available in Tables S1 and S2. This study does not include sex- and gender-based analyses.

(1) All samples were used with the patient's written informed consent in accordance with the Declaration of Helsinki. Clinical data associated with FFPE tumor samples were collected according to the MR-004 guidelines of the CNIL under the registration number n°22_5837.

Cell culture

For 2D studies, HPK were isolated from adult male or female skin biopsies obtained from abdominal reductive surgeries (Genoskin, Toulouse, France) with the informed consent of the donors in accordance with the Declaration of Helsinki (permit AC-2011-1443 from the French Ministry of Higher Education and Research). For HRS, HPK and human primary fibroblasts were isolated from young patients' foreskins obtained with informed consent (Contract 17092C, Children Hospital, Toulouse, France).

Skin samples were washed in Hank's Balanced Salt Solution (HBSS, Sigma-Aldrich) supplemented with 100 UI/ml penicillin, 100 μg/mL streptomycin (Sigma-Aldrich) and 0.5 μg/mL Fungizone (ThermoFisher Scientific). Fat-free skins were cut into small pieces and incubated overnight at 4°C in HBSS containing 10 mg/mL Dispase II (Sigma-Aldrich). The epidermis sheets were recovered, incubated 15 min at 37°C in 0.05% Trypsin-EDTA (ThermoFisher Scientific) and recovered in complete Dulbecco's Modified Eagle Medium (DMEM) containing GlutaMAX-I, 4.5 g/L D-glucose (ThermoFisher Scientific), 10% Fetal Bovine Serum (FBS, Dutscher), 100 UI/ml penicillin and 100 μg/mL streptomycin. HPK were pelleted by centrifugation (1,500 rpm for 5 min) and grown in Dermalife K medium (Cellsystems) supplemented with 100 UI/ml penicillin and 100 μg/mL streptomycin, with medium changes thrice a week. Experiments were performed on low passage ($\leq$3) keratinocytes.

To isolate fibroblasts, small skin pieces were incubated with 1 mg/mL Collagenase H (Sigma-Aldrich) 30 min upon agitation at 37°C. The cell suspension was filtered through a 100 μm nylon cell strainer and centrifuged 10 min at 1,200 rpm. Fibroblasts were grown in complete DMEM medium for 3–6 passages.

The human melanoma WM35 cells were from Dr. M. Herlyn (The Wistar Institute, Philadelphia, PA). SbCl2 and 451Lu cells were provided by Dr. S. Tartare-Deckert (Université Nice Sophia-Antipolis, Inserm, Center Méditerranéen de Médecine Moléculaire, Nice, France). M249 cells were from Dr. R.S. Lo (University of California, Los Angeles, CA). A375, G361, WM1552C and WM266-4 cells were from ATCC (LGC). Melanoma cells were authenticated by STR profiling (Eurofins Genomics). The primary melanoma cell lines (WM35, SbCl2 and WM1552C) were grown in a medium containing 80% MCDB153 medium (Sigma-Aldrich) with 17.86 mM NaHCO3 and adjusted to pH 7.4, 20% Leibovitz's L-15 medium (ThermoFisher Scientific), 1.68 mM CaCl2, 5 μg/mL human insulin (Sigma-Aldrich), 2% FBS, 100 UI/ml penicillin and 100 μg/mL streptomycin. The human metastatic melanoma cell lines (M249, 451Lu, A375, WM266-4 and G361) were grown in RPMI (M249) or DMEM medium supplemented with 7% (451Lu) or 10% FBS and 100 UI/ml penicillin and 100 μg/mL streptomycin. Melanoma cell lines were used for a limited number of passages after thawing and were regularly tested for the absence of mycoplasma contamination by PCR. All cells were grown in the presence of 5% CO_2 in a humidified atmosphere at 37°C.

Construction of SK1 and SK1^{G82D} cell lines

The pcDNA3 plasmids carrying human wild-type *SPHK1* and mutated *SPHK1^{G82D}* sequences were from Dr. S. Pitson (Hanson Institute, Adelaide, Australia). The cDNAs encoding SK1 or SK1^{G82D} were sub-cloned, in replacement of LucR sequence, into the lentiviral pTRIP-DU3-CMV-LucR-2A-eGFP plasmid derived from the self-inactivating lentiviral plasmid pTRIP-DU3-EF1a-eGFP.[54] The constructions were validated by DNA sequencing (Eurofins Genomics Sequencing GmbH, Köln, Germany). Lentiviral particles were prepared by the vectorology facility of the Toulouse Cancer Research Center (CRCT). Briefly, 293FT cells, at 80% confluency in T75 flasks, were co-transfected using calcium phosphate with 10 μg of the pTRIP-CMV-Ctrl, *SPHK1* or *SPHK1^{G82D}* transfer vector plasmid, 10 μg of the p8.91 packaging plasmid and 5 μg of the pVSVg envelope plasmid. Six hours later, the medium was replaced by 12 mL of basal OptiMEM medium (ThermoFisher Scientific). After 20 h, the conditioned media containing lentiviral particles were collected, cleared by centrifugation, filtered through 0.45 μm-pore-size PVDF filters and stored at −80°C.

Melanoma cells were transduced with lentiviral particles during 6 h (MOI 5) in basal OptiMEM medium with 5 μg/mL protamine sulfate (Sanofi-Aventis, France), before growth in complete medium. Shortly after transduction, highly eGFP-expressing cells were sorted on a BD FACSMelody Cell Sorter (BD Biosciences) to ensure homogeneous SK1 and SK1^{G82D} expression. Cell line stability was regularly controlled by FACS analysis.

3D human reconstructed skin (HRS)

The HRS, prepared as previously described,[55,56] were devoid of exogenous materials, composed of a thick dermis rich in endogenous extracellular matrix and a stratified, terminally differentiated epidermal compartment in which CM cells exhibit the same progression behavior as in the patient's skin.[56] Briefly, foreskin fibroblasts were seeded in 24-well plates (50,000/well) and grown for 4 weeks in DMEM medium containing 10% FBS, 100 UI/ml penicillin, 100 μg/mL streptomycin and 50 μg/mL ascorbic acid (Sigma-Aldrich) to form cellular sheets. HPK and Ctrl, SK1 or SK1^{G82D} expressing CM cells were then seeded (200,000 and

50,000 cells/well, respectively) onto fibroblast sheets in Dermalife K medium. After 48 h, three sheets of fibroblasts and one sheet of HPK/melanoma cells/fibroblasts were stacked, lifted to the air-liquid interface for epidermis differentiation and cultured in 3:1 DMEM:Ham's F-12 medium (ThermoFisher Scientific) supplemented with 10% FBS, 0.4 μg/mL hydrocortisone (Sigma-Aldrich), 5 μg/mL bovine insulin (Sigma-Aldrich), 10^{-10} M cholera toxin (Sigma-Aldrich), 100 UI/ml penicillin, 100 μg/mL streptomycin and 50 μg/mL ascorbic acid. Media were changed three times a week. HRS were maintained in culture for two weeks. HRS samples were fixed in 4% paraformaldehyde (ChemCruz) overnight at 4°C and stored in ethanol 70% until paraffin-embedding.

METHOD DETAILS

Sphingolipidomic analyses

Sphingolipid extracts fortified with internal standards were prepared and analyzed by UPLC-TOF MS,[57] except for S1P, which was analyzed as follows. Analysis of the extracts was performed with a system consisting of Acquity ultraperformance liquid chromatography (UPLC) (Waters) connected to a triple-quadrupole mass spectrometer (Xevo TQ-S, Waters) and controlled by Waters/Micromass MassLynx software. Detection was performed with an electrospray interface operating in the positive ion mode, capillary voltage set to 3.1 kV, source temperature at 150°C and desolvation temperature at 500°C. The following selected reaction monitoring transitions were acquired: C17 D-*erythro*-dihydrosphingosine-1-phosphate, 368-252 Da, cone voltage 30 V, collision energy 20 eV; and S1P, 380–264 Da, cone voltage 30 V, collision energy 20 eV.

SK1 enzymatic assay

200 μg cellular extracts were incubated with the following buffer (20 mM Tris (pH 7.4), 20% glycerol, 1 mM mercaptoethanol, 1 mM EDTA, 1 mM sodium orthovanadate, 40 mM β-glycerophosphate, 15 mM NaF, 10 mg/mL leupeptin, 10 mg/ml aprotinin, 10 mg/mL soybean trypsin inhibitor, 1 mM phenylmethylsulfonyl fluoride, and 0.5 mM 4-deoxypyridoxine; Sigma-Aldrich) and 1 mM D-*erythro*-sphingosine (dissolved in 5% Triton X-100; Biomol). Mixed reactions were started by addition of [γ-^{32}P] ATP (10 μCi; PerkinElmer) and 20 mM ATP (Sigma-Aldrich) containing 200 mM MgCl2 and incubated for 30 min at 37°C. Reactions were terminated by addition of 1 N HCl followed by chloroform/methanol/HCl (100:200:1, v/v). After vigorous vortexing, 240 μL of chloroform and 240 μL of 2 M KCl were added, and phases were separated by centrifugation. The ^{32}P-labeled lipids in the organic phase were resolved by thin-layer chromatography on Silica Gel G60 with 1-butanol/methanol/acetic acid/water (80:20:10:20, v/v) and visualized by autoradiography. The radioactive spots corresponding to authentic S1P were identified, scraped from the plates, and quantified using a scintillation counter. Sphingosine kinase specific activity was expressed as pmol of S1P formed per min/mg of protein.

S1P secretion

Melanoma cells cultured in six-well plates were incubated with D-*erythro*-[3-3H]sphingosine (0.45 μCi; Isobio) and D-*erythro*-sphingosine (1.5 μM final concentration; Biomol) for 30 min at 37°C. After labeling, cells were washed with ice-cold PBS and incubated with fresh basal medium for 1 h at 37°C. Alkaline chloroform-methanol extraction was used to isolate lipids from the medium and cells. The radiolabeled S1P contained in the aqueous phase was quantified by liquid scintillation counting. Data were expressed as pmol S1P/mg cell proteins.[58]

CM cell growth

Modified melanoma cell lines were seeded onto 96-well plates in their medium (10,000/well). Twenty-four hours later, cells were treated or not with S1P and monitored for growth during 5 days in an IncuCyte S3 Live-Cell system (Sartorius) using the IncuCyte Cell-by-Cell Analysis software module. The ratio between the number of cells at the end and the number of cells at the beginning of the exponential growth phase was calculated using Microsoft Excel for each condition.

Immunochemistry of HRS

Tyrosinase immunohistochemistry was performed using the automated AS48 (Agilent Technologies) platform. Formalin-fixed paraffin-embedded (FFPE) tissue sections of 5 μm were deparaffinized and heat-pretreated with the PT Link (Agilent Technologies) using the Target Retrieval Solution High pH (pH 8, Agilent Technologies) for 20 min at 95°C. After endogenous peroxidase blocking (10 min, Agilent Technologies), slices were incubated with the mouse monoclonal anti-Tyrosinase antibody (1:100, clone T311, Agilent) in Envision Antibody Diluent, Agilent Technologies) for 30 min. The target was then visualized using the Envision HRP secondary detection system using DAB as a chromogen (K5007, Agilent Technologies). Slices were subsequently counterstained using hematoxylin Link (K800821, Agilent Technologies). The slices were then dehydrated (ethanol and xylene) and mounted using xylene-based mounting. Sections were digitized using a Pannoramic 250 Flash II whole-slide scanner (3DHISTECH, Hungary) in transmitted light mode at a 0.22 μm/pixel resolution. The distances between basal membrane and melanoma cells were evaluated using CaseViewer software (3DHISTECH Ltd).

Cell motility assays

For CM cell motility in co-culture, HPK were seeded onto 96-well plates (10,000/well) in Dermalife K medium 24 h before CM cells. The medium was replaced by CM cells (10,000/well) in their respective medium and cells were co-cultured 24 h before treatment. For

E-cadherin blocking experiments, melanoma cells were incubated or not with an E-cadherin blocking antibody (5 μg/mL; SHE78-7, ThermoFischer Scientific) or an isotypic antibody, for 30 min at 37°C, before being added onto HPK. Otherwise, CM cells were seeded in the absence of HPK. Cell motility was monitored during 3 days in an IncuCyte S3 Live-Cell system (Sartorius). Phase-contrast and green-fluorescent images were acquired hourly (10× objective). For each condition, 40 cells were manually tracked by their eGFP fluorescence over 72 h using the ImageJ plugin "Manual tracking" (Fabrice Cordelières, Institut Curie, Orsay, France) and their motility (μm/min) was measured. Projections of trajectories were plotted using Microsoft Excel.

Wound healing assay

HPK were prelabeled for 30 min with Cell tracker Orange CMTMR (5 μM; ThermoFischer Scientific) and seeded onto an eight-well chamber slide (μ-Slide 8-Well IbiTreat, Ibidi) containing culture-inserts (Ibidi, 45,000 cells/chamber). On the next day, 45,000 melanoma cells labeled with CFSE (Sigma) were seeded in their medium on HPK for 6 h. After removing the inserts, HPK and melanoma cells were co-cultured in the presence of Mitomycin C (0.5 μg/mL; Sigma-Aldrich) and concomitantly treated or not as indicated. Migration was followed every 30 min using an AxioObserver Z1 (Zeiss) videomicroscope during 35 h in a humidified atmosphere of 5% CO_2 at 37°C. CM cells present in the wound were quantified using a Fiji macro based on the « cell counter » plug-in.

Treatments

D-*erythro*-Sphingosine-1-phosphate (S1P, Matreya LLC) was dissolved in methanol. After evaporation, the S1P was resuspended extemporaneously at a final concentration of 10 μM by sonication in basal media containing 4 mg/mL fatty acid-free BSA (Sigma). The S1PR antagonists W146 (Sigma-Aldrich), JTE-013 (Sigma-Aldrich) and CAY10444 (Cayman Chemicals), the proteasome inhibitor MG132 (Selleckchem) and the MMP inhibitor Batimastat (Sigma-Aldrich), the MEK inhibitor Trametinib (MedChemExpress) and the PI3K inhibitor GDC-0941 (Axon Medchem) were solubilized according to the supplier recommendations.

RNA-sequencing

HPK were seeded in T75 flasks (400,000 cells/flask) and grown until 80% confluency before treatment. Libraries were prepared from 1000 ng total RNA using the Truseq Stranded mRNA Kit and IDT for Illumina Truseq RNA UD Indexes from Illumina. Libraries size and quality were confirmed on Fragment Analyzer (Agilent). KAPA quantification kit for Illumina platforms (KAPA Biosystems, Roche) was used to quantify librairies by qPCR. Barcoded libraries were equimolar pooled and pair end sequenced (2 × 76bp) on the Illumina NextSeq 550 instrument using high output V2.5 kit (Illumina). Biological replicate concordance was assessed using principal component analysis. Duplicated genes were averaged. Low-expressed genes were filtered out by applying the following criterion: estimated counts (from RSEM) > 5 for at least 3 samples. Filtered estimated read counts from RSEM were compared using the R Bioconductor package DESeq2 v1.38.3 based on generalized linear model and negative binomial distribution.[59] Genes with Benjamini–Hochberg corrected p value <0.01 were selected as differentially expressed genes. Gene-set enrichment was done using fgsea package. Heatmap was done using ComplexHeatmap[60] and volcanoplot/barplot were done using ggplot2.[61]

Flow cytometry

CM cells were seeded in T25 flasks (500,000 cells/flask) 24 h before experiment. Cells were dissociated in PBS containing 2 mM EDTA for 15 min at 37°C and were sequentially labeled with an anti-E-Cadherin monoclonal antibody (1:1,000, clone E700Y, Abcam) for 1 h and an Alexa Fluor 647 goat anti-rabbit antibody (1:500, Invitrogen) with DAPI (0.5 μg/mL) for 30 min at 4°C, in PBS 2 mM EDTA 1% BSA. Cell labeling was measured on an LSRII cytometer (BD Biosciences) and analyzed with BD FACSDiva v9.0.1 and FlowJo v10.8.1 softwares.

Cell adhesion assays

HPK were seeded in 96-well plates (50,000 cells/well) 24 h before the experiment. After treatment of HPK with S1P, the medium was replaced with CFSE-labeled melanoma cells (10,000 cells/well) in adhesion buffer (PBS 1% BSA and 1 mM $CaCl_2$). After incubation for 1 h at 37°C, non-adherent cells were removed and wells were gently washed once with adhesion buffer. For blocking experiments, CFSE-labeled melanoma cells were incubated or not with an E-cadherin-blocking monoclonal antibody (7.5 μg/mL; SHE78-7, ThermoFischer Scientific) or an isotypic antibody, 30 min at 4°C, before being added onto HPK. Adherent melanoma cells were quantified by fluorescence microscopy (AxioVert, Zeiss) on one central field per well (5× magnification) using the « cell counter » plug-in or with the Operetta CLS high-content analysis system using the Harmony high-content imagining and analysis software (PerkinElmer). For accurate quantification, the numbers of CM cells on S1P-treated or untreated HPK were compared between immediate neighbor wells.

Immunofluorescence staining of 2D samples

HPK or CM cells were seeded onto eight-well chamber slides (μ-Slide 8-Well ibiTreat, Ibidi) (50,000 HPK/chamber) or coverslips in 24-well plates (50,000 CM cells/well), respectively, 48 h before treatment. Cells were fixed with 4% paraformaldehyde for 10 min at room temperature (RT), blocked and permeabilized with PBS 5% BSA 0.1% saponin (Sigma-Aldrich) for 20 min and incubated sequentially with an anti-E-cadherin antibody (1:200, clone 24E10, Cell Signaling Technologies) for 2h and an Alexa Fluor 546 conjugated anti-rabbit antibody (1:500, Life Technologies) with 4,6-diamidino-2-phenylindole (1:1,000, DAPI) for 30 min. Cells were

washed, covered with Vectashield (Eurobio Scientific), and visualized using an LSM 780 Confocal (Zeiss) microscope. The fluorescence intensity of E-cadherin per cell was calculated using ImageJ software.

Quantitative RT-PCR

HPK were seeded in T75 flasks (400,000 cells/flask) and grown until 80% confluency before treatment. RNA was extracted (RNeasy Kit Plus; Qiagen). RNA quality was assessed by automated gel electrophoresis (Experion; Bio-Rad). One microgram of RNA was reverse transcribed (SuperScript II; Invitrogen) and the cDNA used as a template for qPCR. The reactions were performed in duplicate on the StepOne instrument (Applied Biosystems) using SYBR Green PCR Kit and primer assay (QuantiTect, Qiagen). Results were quantified using the StepOne system software and normalized with respect to GAPDH and β-actin transcripts. The qPCR primers were from Qiagen: CDH1 (QT00080143), SNAI1 (QT00010010), SNAI2 (QT00044128), TWIST1 (QT00011956), ZEB1 (QT00020972), ZEB2 (QT00008554), GAPDH (QT00079247), ACTB (QT00095431).

Western blot analyses

HPK were seeded in T75 flasks (400,000 cells/flask) and grown until 80% confluency before treatment. CM cells (1,000,000 cells/flask) were seeded 24h before treatment. Cells were lysed with Cell Lysis Buffer (Cell Signaling Technology) and sonicated. Proteins were separated by electrophoresis on SDS-PAGE, transferred onto a nitrocellulose membrane (PerkinElmer) and revealed with monoclonal anti-E-cadherin (1:10,000, clone 24E10), anti-Snail (1:1,000, clone C15D3), anti-Slug (1:1,000, clone C19G7) or anti-β-Actin (1:1,000, clone 13E5) (Cell Signaling Technology). Proteins were detected using an ECL detection system and Chemidoc imager (Bio-Rad) and quantified using ImageLab software (Bio-Rad). β-Actin was used for normalization.

Preparation of conditioned medium

CM cells were seeded in T75 flasks (500,000 cells/flask) 24 h before medium replacement with Dermalife K medium. The conditioned media were collected 48 h later and centrifuged at 1,500 rpm for 3 min at 4°C. The supernatants were stored at −80°C.

Quantification of MMP secretion by zymography

HPK were seeded in T75 flasks (500,000 cells/flask) and grown for 48 h in Dermalife K medium. Then, HPK were starved for 24 h in Dermalife basal medium (Cellsystems) before treatments. After treatments, supernatants were collected, centrifuged at 500 g for 5 min at 4°C, and concentrated at least 20 times using Vivaspin6 10.000 MWCO (Sartorius), 4,000 g, 4°C before storage at −80°C and analysis within 14 days. Cells were harvested and counted. Concentrated supernatants were incubated for 15 min at RT with 3x non-reducing sample loading buffer containing 188 mM Tris-HCl buffer pH 6.8, 6% (w/v) SDS, 0.03% (w/v) bromophenol blue and 30% (v/v) glycerol. Samples were then separated on a 1 mm 7.5% polyacrylamide gel containing 1 mg/mL Gelatin from Porcine skin (Sigma). Sample loading was corrected for total cell count and the concentration factor of the conditioned media. After electrophoresis, the gel was washed in water twice and thereafter washed 4 times 15 min at RT in 50 mM Tris-HCl buffer pH 7.6 with 2% (v/v) Triton X-100 (Sigma). Subsequently the gel was incubated for 30 min at RT and 24 h at 37°C in 50 mM Tris-HCl buffer pH 7.6 with 5 mM CaCl2 dihydrate and 150 mM NaCl. During the removal of SDS and the described incubation, pro-MMPs become partially refolded, and autoactivate, allowing the detection by zymography of a pro-MMP portion of the originally inactive pro-MMPs. Lastly the gel was stained by 0.5% (w/v) Coomassie brilliant blue R-250. Pictures were taken from the gels and quantified using ImageJ.

Immunohistochemistry of melanomas

Serial three-μm tissue sections were cut from FFPE human melanoma specimens. Sections underwent immuno-histochemical staining with an antibody against SK1 (1:500, ab260073, Abcam), on a Leica Bond RX. Melanoma samples were classified following their SK1 expression by a pathologist.

Immunofluorescence of HRS and melanomas

HRS and melanoma sections underwent immunofluorescence staining using the Opal 6-Plex Manual Detection Kit (Akoya Biosciences) on a Leica Bond RX. Epitope retrieval was carried-out using BOND Epitope Retrieval Solution 2 (EDTA, pH9) (Leica Biosystems). A 2-color panel included labeling of SOX10 (1:1,000, sc-365692, Santa Cruz) and E-Cadherin (1:4, 790–4497, Ventana). DAPI was used for nuclei detection. Sections were digitalized with a Vectra Polaris scanner (PerkinElmer, USA). An autofluorescence treatment of images and the phenotyping were carried out using the inForm Advanced Analysis software (PerkinElmer).

Samples were tissue-segmented for tumor ($SOX10^+$), epidermis ($E\text{-cadherin}^+$ and $SOX10^-$) and stroma ($SOX10^-$ and $E\text{-cadherin}^-$). Cells were phenotyped ($SOX10^+$ $E\text{-cad}^-$, $SOX10^-$ $E\ cad^+$ or $SOX10^-$ $Ecad^-$) and segmented. Scores reporting individual features for each cell (fluorescence intensity of each fluorochrome in nucleus, cytoplasm and membrane, phenotype, tissue localization and spatial coordinates) were analyzed using the R software. Interactive plots linking scores to cell localization were developed using the R package Shiny.

For epidermal E-cadherin quantification in HRS, membrane E-cadherin fluorescence intensities were collected from 10 basal keratinocytes in 5 regions of interest (ROIs) proximal to tumor cells and 5 ROI distant from tumor cells. Membrane E-cadherin intensity of each proximal keratinocytes was reported to the mean of E-cadherin intensity in distal keratinocytes. For tumor E-cadherin quantification, individual membrane fluorescence intensities were monitored from 10 $SOX10^+$ CM cells in 5 proximal ROI. Representative

images were acquired using a confocal LSM 880 FAS Airyscan microscope (Zeiss). 3D structures were obtained with Imaris 9.9.1 (Bitplane, Belfast, UK). All images were first converted from Zen format (.czi) into "Imaris Image Files" with Imaris File Converter.

For epidermal E-cadherin quantification in melanoma samples, membrane E-cadherin fluorescence intensities were collected from a distant and a proximal ROI (ROI size, 925 × 694 μM, separated by 3361 μm +/− 2677 μm and 3882 μm +/− 2972 μm, for $SK1^{low}$ and $SK1^{high}$ melanomas respectively). For each specimen, the mean of E-cadherin intensity in the proximal ROI was reported to the mean of E-cadherin intensity in the distal ROI. For tumor E-cadherin quantification in melanoma samples, the mean of membrane E-cadherin fluorescence intensity of $SOX10^{+}$ CM cells was determined from 3 ROIs located at the edge, surface and center of the tumor. Representative images were extracted from images obtained with a Vectra Polaris scanner using Phenochart.

QUANTIFICATION AND STATISTICAL ANALYSIS

All statistical analyses, except RNA-seq analyses, were performed using GraphPad Prism 9.4.1 software and are included in the figure legends. Results were expressed as mean or median ±SEM from three independent experiments except when indicated. Two group comparisons were performed with unpaired or paired Student's t-tests or Mann-Whitney (unpaired) or Wilcoxon (paired) tests if Shapiro-Wilk test of normality was not achieved. For comparison of three or more groups, one-way ANOVA followed by Tukey's, Holm-Šídák's or Dunnett's post hoc test, or Kruskal-Wallis followed by Dunn's post hoc test were performed if Shapiro-Wilk test of normality was not achieved. When necessary, two-way ANOVA tests with post hoc Bonferroni's test were used. Correlations were assessed using Pearson's correlation coefficient. A p value inferior to 0.05 was considered statistically significant (ns, not significant; *, $p < 0.05$; **, $p < 0.01$; ***, $p < 0.001$; ****, $p < 0.0001$).